NTNU

Norwegian University of
Science and Technology

Community structure and biodiversity of the benthic megafauna at the inactive hydrothermal site Mohn's Treasure, on the Mohn's Ridge, Arctic Mid-Ocean Ridge (AMOR)

Emil Paulsen

Acknowledgements

List of Abbreviations

AMOR	-	Arctic Mid-Ocean Ridge
AVT	-	Allied vision technologies
BIOFAR	-	Biology of the Faroe Islands
BIOICE	-	Benthic Invertebrates of ICElandic waters
CCD	-	Charge-coupled device
CSV	-	Construction support vessel
EEZ	-	Exclusive economic zone
FOV	-	Field of view
GIF	-	Greenland – Iceland – Faroe Ridge
H'	-	Shannon – Weaver diversity index
ICES	-	International Council for the Exploration of the Sea
J	-	Pielou's evenness index
JMVF	-	Jan Mayen vent field
LCVF	-	Loki's Castle venf field
MAR	-	Mid - Atlantic Ridge
MV	-	Mud volcano
NSDW	-	Norwegian Sea Deep Water
ROV	-	Remotely operated vehicle
SD	-	Standard deviation
SMS	-	Seafloor massive sulphide
S – W	-	Shannon-Weaver
UiB	-	University in Bergen
VF	-	Vent field
VT	-	Video transect
VME	-	Vulnerable marine ecosystem

Sammendrag

Denne masteroppgaven representerer den første studien av bentisk dyphavs-megafauna på det geologisk inaktive hydrotermale området Mohn's Treasure, lokalisert på den Arktiske Midthavsryggen (AMOR). Geologisk inaktive områder kan potensielt inneholde såkalte *seafloor massive sulphide* (SMS), lokalt forhøyede forekomster av industrielt viktige mineraler som kopper, nikkel, zink, gull og flere andre mineraler. Det har de siste årene vært en økt interesse fra kommersielle aktører for å utforske mulighetene og lønnsomheten av å utvinne disse mineralforekomstene. En eventuell framtidig gruvedrift på havbunnen vil ha store konsekvenser for dyresamfunnene som bor på de aktuelle områdene. Denne påvirkningen vil være i form av fysisk ødeleggelse av habitat, forurensning i form av avfall, og gjennom spredning av løsmasser i de nærliggende områdene. For å forstå de biologiske effektene og konsekvensene av gruvedrift på havbunnen er det helt essensielt å skaffe kunnskap om artene som bor i områder der framtidig mineralutvinning kan være aktuelt.

Geologisk aktive områder med hydrotermale skorsteiner har blitt studert i en årrekke, helt siden de første gang ble oppdaget på slutten av 1970-tallet. Geologisk inaktive områder har imidlertid forblitt ubeskrevet og lite utforsket når det gjelder biologiske faktorer. Denne masteroppgaven representerer den første studien gjort på bentiske megafauna-samfunn på det geologisk inaktive området Mohn's Treasure, og vil fungere som en biologisk introduksjon til området. Den samlede dataen for denne oppgaven består av bildetransekter hentet fra tre distinkte lokasjoner av Mohn's Treasure. Totalt ble 43 ulike taksonomiske grupper observert, og gjennomsnittlig tetthet på hver lokasjon var cirka 30 ind. m^{-2}. De to mest utbredde dyregruppene, både i antall individer og antall arter, er rekkene Porifera og Echinodermata. Områder med bløtbunn er totalt dominert av sjøliljer (Crinoider) av arten *Bathycrinus carpenterii*, mens områder med hardbunn er karakterisert av høye forekomster med svamper fra mange ulike arter.

Abstract

This MSc is the first study to investigate the deep – sea benthic megafauna inhabiting the geologically inactive hydrothermal site of Mohn's Treasure, on the Arctic Mid-Ocean Ridge. Inactive vent sites might represent potential *seafloor massive sulphide* (SMS) deposits, containing localized concentrations of industrial minerals, including copper, nickel, zinc, gold and several more. There is increasing interest in commercial exploration and exploitation of these sites. Especially the latter will have significant impacts on the animal communities inhabiting these locations. Deep sea mining will impact the local fauna through physical removal of habitat, discharge of waste water and via creating sediment plumes. To fully understand the biological consequences of deep sea mining it is crucial to gather knowledge of the species living is areas of future mining.

While geologically active vent sites have been studied for several decades, since their discovery in the 1970s, inactive sites have remained more or less undescribed regarding biological features. This thesis represents the first study of benthic megafauna communities at the inactive site of Mohn's Treasure, and will work as a baseline study. The data gathered by a remotely operated vehicle consists of photographs taken along transects at three distinctive sites at Mohn's Treasure. A total number of 43 taxa have been recorded, and the mean density for each site is approximately 30 ind. m^{-2}. The two most abundant animal phyla, both in number of specimens and number of taxa are Porifera and Echinoderms. The soft sediment is totally dominated by sea lilies (Crinoids) of the species *Bathycrinus carpenterii*, while areas of hard bottom substratum is characterised by high abundances of sponges from a large number of species.

Table of content

List of Tables

List of Figures

1. Introduction

1.1. Oceanography and biological research of the Norwegian Sea

The Nordic Seas (Greenland – Iceland – Norwegian Sea) (Fig. 1) represent the northernmost part of the Atlantic Ocean and constitute the connection to the Arctic Ocean (Oug et al., 2017). The border between the Nordic Seas and the North Atlantic is formed by one of the major topographic features in the area, the submarine ridge between Greenland and Scotland, named the Greenland-Iceland-Faroe Ridge (GIF) (Skjoldal, 2004). Substantial parts of these marginal seas are underlain by deep basins with depths close to 4000m. In depths greater than 700m the water-masses within these basins are more or less homogenous and colder (<0°C) than most other deep-water masses found around the world. The faunas inhabiting Arctic deep waters differ from those of most other deep waters in having a low species diversity, even for the most pronounced of deep-sea taxa. It has been suggested that the young geological age (3my) of the Arctic abyssal fauna could be the cause of this low diversity (Svavarsson et al., 1990).
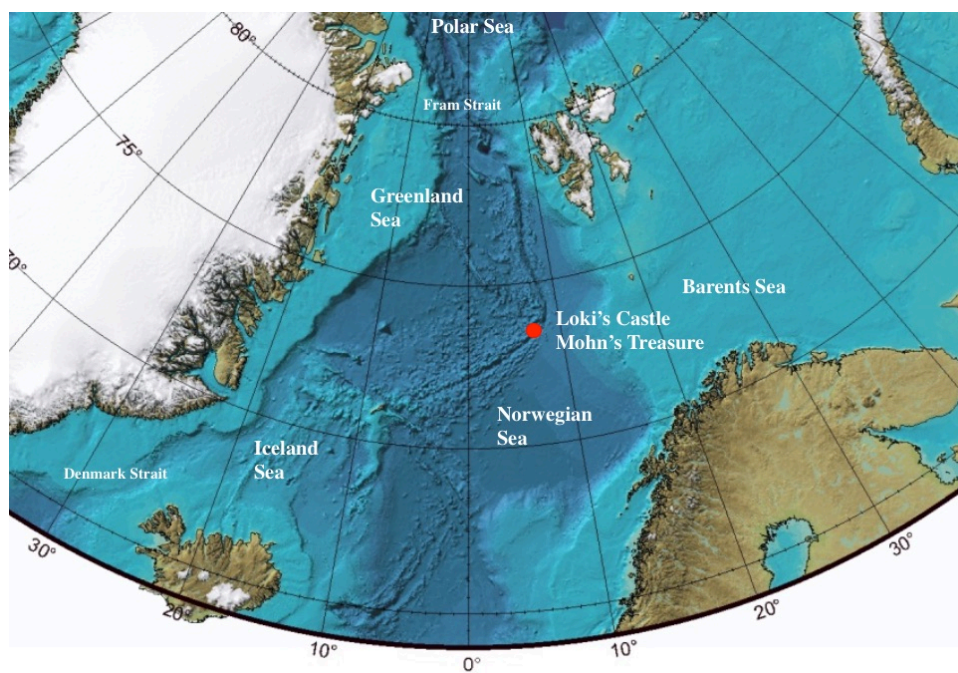
Fig. 1. The Nordic Seas: Norwegian Sea, Iceland Sea and Greenland Sea. The red point shows the location of the geologically active vent site of Loki's Castle at 73°33.97'N 08°09.51'E and the geologically inactive site of Mohn's Treasure. Located 30 km apart, where the Mohn's Ridge bends northwards and becomes the Knipovich Ridge. Modified from Sakshaug, 2009.

The ocean between Greenland and Norway is divided into the Greenland Sea (including the Iceland Sea) and the Norwegian Sea (Fig. 1). The Greenland Sea stretches from the Fram Strait to the Denmark Strait between Greenland and Iceland, and the Norwegian Sea from Svalbard and northern Norway to the GIF ridge (Svavarsson et al., 1990). The GIF ridge breaks the surface in Iceland and the Faroe Islands while the deepest locations are found in the Faroe Bank Channel, south of the Faroes (840m), and in the Denmark Strait (620m) (Fig. 1) (Skjoldal, 2004). The minimum sill depth between the Greenland and Norwegian Seas and the Arctic Sea is at least 2600m (Svavarsson et al., 1990). This sill depth was not examined until the Polar Front Survey in 1958. Then it was observed by a vessel from the Soviet Union (Skjoldal, 2004). The deep basins of the Arctic Ocean are well separated from the abyssal depth of both the North Pacific and North Atlantic Oceans. These basins are mostly 3000 - 4000m deep, separated by ridges that may rise in excess of 1000m above the adjacent abyssal plains (Svavarsson et al., 1990).

The Norwegian Sea Deep Water (NSDW) is the predominant water mass in the two Seas. It is characterized by a uniform salinity of 34,90 – 34,94, and temperatures below 0ºC. It forms during the winter in the centre of the Greenland Sea, sinks into the Greenland Basin and then flows into the Norwegian Sea. Another source of deep water is over the North Polar Sea shelves, from the dense brine water formed due to ice formation (Svavarsson et al., 1990).

The top centimetre of the bottom sediments in the deep basins of the Norwegian and Greenland Seas are composed of:

1. Clay and foraminiferal clays, which occur as a tongue stretching from Scoresby Sound in Greenland towards Svalbard and including the deep Greenland Basin,
2. sandy clay, marl or ooze, which occurs mainly on ocean ridges and in shallower coastal waters, and
3. foraminiferal clay, marl or ooze, which covers most of the deep basins off Norway (Svavarsson et al., 1990).

Whereas the coastal and continental shelf areas have been extensively studied, particularly along the European coasts, the continental slope and deep-water systems (approx. 500 – 4000 m) have received far less attention (Oug et al., 2017). The deep water fauna of the Norwegian Sea was first described in several reports from the *Norwegian North Atlantic Expedition*, 1876 – 1878 (Wille et al., 1882). The immense material of benthic animals from this expedition was described taxonomically by several experts during the following years and even decades. However, a final, biogeographic summary was never published (Høisæter, 2010).

The Danish *Ingolf* Expeditions in 1895/1896 explored waters around the Faroe Islands, Iceland and Greenland. This was the first time a fine mesh was used in the sampling gear to separate the smaller benthic invertebrates from the sediment, leading to discovery of many small macroorganisms (Brix et al., 2014). Other pioneering expeditions aiming to gather information on deep-water marine organisms from the Norwegian Sea include Danish expeditions in the early twentieth century (Oug et al., 2017), and also the 1910 *Michael Sars Expedition* (Høisæter, 2010).

Over half a century later, in 1976, the French/Swedish *NORBI* expedition covered the northern and eastern parts of the Norwegian Sea, at depths from 2500 to 3800 m. Based on work by Bouchet & Warén (1979), who examined molluscan material from this expedition, conclusions were that the benthic fauna of the abyssal (deeper than c. 2500 m) is comparatively species poor. However, it seems to be highly endemic, sharing only a few species with similar depth zones in the North Atlantic south of the GIF Ridge, or the mollusc fauna of the slope shallower than c. 2000 m (Høisæter, 2010). This is further backed up by studies conducted on benthic deep-water fauna in the Norwegian Sea, indicating a sparse deep water fauna of rather low diversity (Oug et al., 2017). These new studies (Høisæter, 2010; Oug et al. 2017) are based on extensive sampling during 1980 – 87 (Sneli 1998, Høisæter 2010), which in addition to the BIOFAR and BIOICE programme also covers the southern part of the Nordic Seas.

The BIOFAR project (*Biology of the Faeroe Islands)* was initiated by Norwegian and Danish marine biologists, and led to extensive new knowledge on benthic invertebrates in the Faroe region (Sneli et al, 2005; Brix et al. 2014). Based on BIOFAR, the international BIOICE (*Benthic Invertebrates of ICElandic waters)* was focused on the collection and characterization of benthic invertebrates within the Icelandic economic zone. Data from the BIOICE project has greatly expanded our knowledge of the benthic invertebrates in this region, their taxonomy, distribution and diversity (Brix et al., 2014).

Studies done on megabenthos gathered from the Atlantic as a whole indicates that diversity increases sharply from upper bathyal depths to about 2000 m and then decline toward the abyss, remaining low from abyssal to hadal depths (Rex et al., 2010). In comparison, the diversity in the Norwegian Sea peaks at shallower depths and then decreases with depth to much lower values than those found in the Atlantic Ocean (Rex et al., 2010). Several taxonomical groups, however, are poorly studied and imperfectly known, and in several cases most relevant information actually dates back to the pioneering expeditions in the nineteenth and early twentieth centuries (Kongsrud et al., 2011). This emphasizes the need of continuous study in these areas.

1.2. Hydrothermal vents

Since hydrothermal vents were discovered in 1977 (Baker et al., 2013), scientific research has been the primary source of anthropogenic disturbance in these ecosystems. However, there is increasing interest in commercial exploration and exploitation of seafloor massive sulphide (SMS) deposits that host vent communities (Van Dover, 2014). These activities represent a whole new level of impact on these unique vent ecosystems, and to make sure we understand the consequences better, sufficient studies need to be at hand.

SMS are large deposits of metal-bearing minerals that occur on and below the seabed. They are formed through precipitation of minerals from hydrothermal fluid, which is made possible due to interactions between seawater and a heat source (magma) in the sub-sea-floor region. During this process, cold seawater penetrates through cracks in the seafloor, reaching depths of as much as several kilometres below the seafloor surface (Petersen et al., 2013). The fluid can reach temperatures up too 400º C, though most hot vents are around 300 - 350 º C. As the heated seawater rises rapidly to the sea floor due to lower density than colder water, it leaches out metals from the surrounding rock. These metals are transported with the water, where most of it is expelled into the overlying water column as focused flow at chimney vent sites. The dissolved metals then precipitate when the vent fluid mixes with the cold and oxyganated seawater, forming the metal deposits and vent chimneys (Petersen et al., 2013).

Hydrothermal chimneys can discharge various colours of smoke, including black, grey, white and yellow. The temperature of the fluid influences the colour of the smoke, through dissolving different compounds at different temperatures. Black smokers have the highest fluid temperature (greater than 330º C), and the particulates are predominantly sulphide minerals (Petersen et al., 2013).

Hydrothermal vents occur in areas of undersea volcanic activitiy, most commonly associated with mid-ocean ridges at plate boundaries (Fisher et. al., 2013). Most sulphide occurrences, as much as 65 per cent, have been found along mid-ocean ridges, with another 22 per cent occurring in back-arc basins and 12 per cent along submarine volcanic arcs. At mid-ocean ridges, such as the Mid-Atlantic Ridge (MAR), venting of high temperature is normally found around the axial zones of the spreading centres and is associated with basaltic volcanism. However, at slow-spreading ridges, like the Arctic Mid-Ocean Ridge (AMOR), fluid flow might be diverted away from the actual ridge axis. This can be caused by detachment faults.

Consequences of this is that the associated sulphide deposits can, in fact, be found several kilometres away from the ridge axis (Petersen et al., 2013).

The extreme temperatures, in addition to high concentrations of chemicals that are toxic to most animals, make it impossible for most species to survive at or close to active vent sites. However, these chemicals are used as an energy source for growth by chemoautotrophic microorganisms (Fisher et al., 2013). Chemoautotrophy is the production of organic matter from CO_2, coupled to a redox reaction. These reactions take place between inorganic chemicals to obtain energy (Sievert et al., 2012). At vent sites the microorganisms use reduces compounds such as H_2 and CH_4 from the vent fluid (Sievert et al., 2012), in reaction with O_2 from the surrounding waters, to synthesise organic matter. These organisms have been found in symbiosis with megafauna, and as free living forming bacterial mats on the hydrothermal vents. There are over 400 animal species described from vents, many of which are vent-endemic. They have evolved a symbiotic, or mutually beneficial, relationship with chemoautotrophic bacteria, which allows them to benefit directly from the energy in hydrothermal vent fluids and some places reach densities of hundreds to thousands of individuals per square meter (Fisher et al., 2013).

1.3. AMOR vents

The slow to ultraslow spreading Arctic Mid-Ocean Ridge (AMOR) (Pedersen et al, 2010), extends from the northern shelf of Iceland to the Siberian Shelf in the Laptev Sea (Baumberger et al 2016), and makes up the tectonic boundary between the North American Plate and the Eurasian Plate (Fig. 2). In the area of the Norwegian Sea and the Greenland Sea the AMOR consists of the Kolbeinsey Ridge and the Mohn's- and Knipovich Ridges (Olsen et al, 2015) (Fig. 2). The spreading speed of the AMOR ranges from 55 mm per year to less than 20 mm per year. At spreading speed less than 20 mm per year, volcanic activity decreases to a level where the crust becomes thinner than normal and may even disappear. It has been questioned if hydrothermal activity could at all be present at these sites, but the relatively recent discoveries of black smokers at ultraslow spreading ridges has shown that venting is more common than expected (Edmonds et al., 2003; Pedersen et al., 2010).

Several active and inactive hydrothermal systems have been discovered along the AMOR, where the fields are located within the Norwegian EEZ or at the Extended Continental Shelf. So far two inactive and four active hydrothermal systems have been detected at the Kolbeinsey Ridge and the Mohn's- and Knipovich Ridges (Fig. 2) (Olsen et al, 2015).
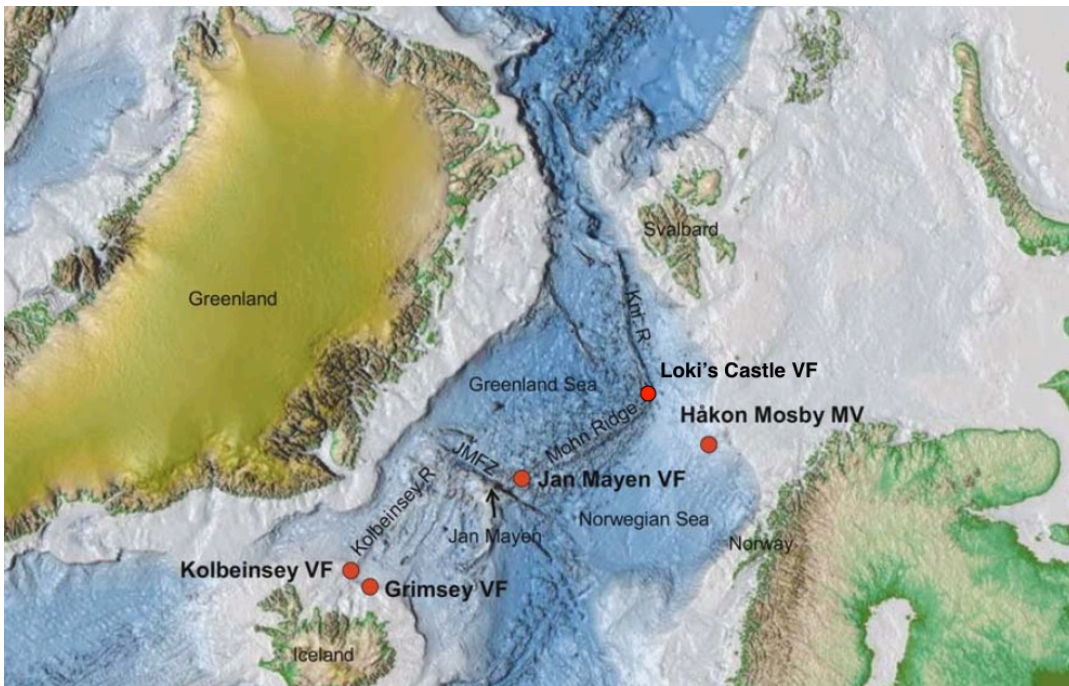
Fig. 2. Geological activity in the Nordic Seas. Showing how the Arctic Mid-Ocean Ridge, consisting of the Mohn's Ridge and the Knipovich Ridge stretches from Island and nortwards on the western side of Svalbard. Red points show the location of discovered vent fields (VF) and the Håkon Mosby mud volcano (MD). (JMFZ) Jan Mayen Fracture Zone. Modified from Schander et al., 2010.

The first vent field discoveries at the AMOR were done in 2005 during a cruise by the University of Bergen (UiB). They discovered the Jan Mayen vent field (JMVF) at the Mohn's Ridge at 71º N (Fig. 2). It consists of at least three high-temperature vent fields: Soria Moria,

Troll Wall and Perle and Bruse. The fields are found between 500 and 700 m depth have white smokers emanating fluids with temperatures up to 270º C (Olsen et al, 2015). Three years later, in 2008, another cruise by UiB found the Loki's Castle vent field (LCVF) located at 2400 m depth at 73º N 8º E, where the Mohn's Ridge passes into the Knipovich Ridge (Fig. 1, Fig. 2) (Pedersen et al, 2010). Loki's Castle represents the first known deep black smoker vent system in the Arctic region (Pedersen et al, 2010) and is perhaps the most ground-breaking discovery made during the investigations along the AMOR so far (Rapp, 2015).

The discovery of LCVF on the AMOR represented the first black smoker vent system ever found on such slow spreading ridges. Further it was also the first recorded true vent-endemic fauna along the AMOR. Studies show that the fauna differs from the surrounding deep-sea communities. A preliminary characterization suggests two zones;

1. black smoker chimneys with microbiota, but also gastropods and amphipods, and
2. low-temperature venting with barite chimneys.

The first is hard bottom substrata with sparse fauna biomass, highly variable in abundance and generally low in diversity. The second is primarily a soft bottom habitat with quite diverse and abundant fauna. Characteristic organisms are siboglinid tubeworms (*Sclerolinum contortum*), amphipods, gastropods and tube dwelling polychaetes (Olsen et al, 2015).

The fauna at Atlantic vent sites is distinct from that at Pacific sites, and East Indian Ridge vents seems to be a mix of both. Based on these preliminary data, it has been suggested that the ridge may be used as a stepping stone pathway for dispersal of vent organisms, connecting the Pacific and the Arctic/Atlantic oceans (Pedersen et al., 2010). In this sense Iceland forms a geographic barrier for northward along-ridge migration (Pedersen et al, 2010). This is also pointed out by Schander et al. (2010) who proposes that Iceland and the *Greenland-Iceland-Faroe Ridge* prevents larvae from spreading from the Mid-Atlantic Ridge (MAR) to the northern areas. It is further reported that Loki's Castle supports a vent fauna that is different from that found further south in the Atlantic, where shrimps, large bivalves and crabs are abundant. This has led to the suggestion that the fauna at Loki's Castle is locally adapted and has phylogenetic links to vent fauna from the Western Pacific and from Arctic cold seeps (Pedersen et al, 2010), being isolated from the MAR fauna by Iceland. There are ongoing studies at these sites, and the published work concentrates mainly on the firste description of the LCVF (Pedersen et al., 2010), microbiology (Spang et al., 2015; Steen et al., 2016) and on the taxonomy of specific fauna (Tandberg et al., 2011; Kongsrud et al., 2012).

The fauna of the Mohn's Ridge vent fields seems to have more in common with the Håkon Mosby seep fauna than with any of the other Atlantic vent field faunas. This may be explained by the small geographic distance between the Mohn's Ridge and the Håkon Mosby mud volcano (Fig. 2), the currents and the dominating water masses (Schander et al. 2010). It is further pointed out that there is little difference in faunal composition between surrounding waters and the actual vent fields in the Mohn's Ridge. All the studied animal groups show an assemblage very similar to what is usually found at comparable depths in the surrounding waters. This indicates that key environmental variables such as temperature, salinity, current speed and direction, resuspension of sediments may be more important factors in this region

then the actual venting. It is also pointed out that it is not a simple factor that affects current composition of the fauna of the hydrothermal vent fields on the northernmost Atlantic/Arctic Mid-Ocean Ridge, and that we still know very little about the amount of venting in the northern part of the AMOR (Schander et al, 2010). This emphasizes the need for continuing exploration of these ridge areas, both to better understand the vent fields, but also their surrounding and less geologically active areas.

1.4. Geological inactive vent sites

The geologically inactive site of Mohn's Treasure at 73°N 07°E, around 2600 m depth, is found approx. 30 km to the south-west of Loki's Castle (Fig. 2, Fig 3). It is located at the edge of an inner rift wall suggested by Olsen et al. (2015) to be a mass-wasting feature made up of partly lithified sediments. Mohn's Treasure consists of fine-grained porous chimney fragments with fluid channels and is predominantly composed of pyrite (Olsen et al, 2015). The seabed for abyssal depths close to a ridge, like Mohn's Treasure is typically characterised by large areas of soft sediment, with varying degrees of rocky outcrops (Ramirez-Llodra et al., 2010). Inactive vent sites have no detectable emissions of hydrothermal fluids and, although poorly studied to date, often hosts suspension-feeding and grazing invertebrates that may also occur on rock outcrops not formed by hydrothermal mineralization (e.g. basalt) (Van Dover, 2010).

Knowledge on the biological composition and ecological functions of faunal communities at inactive sites is still utterly scarce, and there is no biological information from Mohn's Treasure yet. Some investigations have been conducted at the inactive sulphide deposit in Manus Basin, just off the north-east coast of Papua New Guinea. This indicates that in that location, inactive sulphides and other hard substrata are colonized by suspension-feeders (e.g. corals, barnacles, sponges) that depend on chemosynthetic production. This production is most likely advected from nearby active vent systems (Van Dover, 2010).

1.5. Deep-sea mining

Over the last half-century metal grades in terrestrial mineral deposits are reported to be decreasing steadily (Rodgers, 2013). Triggered by growing demand, there has been a progressive increase in metal prices. This, combined with technological improvements regarding mining, exploitation of massive low-grade deposits are now becoming economical. However, mining these deposits, which often occur in remote and challenging terrain, produce

large volumes of waste material that can cause environmental degradation if poorly managed. Factors such as these have turned the attention of investors and developers to alternative sources of metals, including deep sea. The existence of minerals on the seabed has been known for many years and there have been numerous research cruises aimed at understanding and documenting these potentially rich deposits. They represent a potential source of important industrial minerals, including copper, nickel, zinc, gold, silver, manganese, cobalt, molybdenum, rare-earth elements, and others (Rodgers, 2013).

The deep sea mineral resources that have been discovered today can be divided into three main groups:

1. Sea-floor massive sulphide (SMS) deposits – which form at hydrothermal vents and contain localized concentrations of copper, lead and zinc, with significant amounts of gold and silver,
2. manganese nodules found at certain abyssal plain, and
3. cobalt-rich ferromanganese crusts that form on active seamounts, containing notable concentrations of nickel, copper and cobalt, coupled with significant concentrations of rare-earth and other rare metals (Baker et al., 2013).

The deep - sea mineral resources explored at the AMOR is the first group, SMS deposits. While the exploitation of these deposits are, at best, many years into the future yet, mining is expected to involve the following basic operations;

1. Extraction of minerals from the sea floor using remotely operated sea-floor production equipment,
2. transport of a slurry or ore and seawater vertically from the sea floor to a vessel or platform on the sea surface,
3. dewatering of the ore on board a vessel or platform,
4. transfer of the ore from the vessel to a transport barge or bulk carrier/storage facility (silo vessel offshore or land-based) and disposal of the separated seawater and
5. transport of the ore to land treatment and/or processing (Smith et al., 2013).

Like any mining project disaggregating the minerals on the sea floor will result in the physical removal of habitat and animals. This is likely to cause loss of habitat for some faunal groups. SMS mining will reshape the sea floor, removing vertical edifices and altering the texture of the substratum.

Another important impact can be the creation of a sediment plume through dispersal by currents. This will leave a larger footprint than the physical mining area. The same goes for the area affected by discharge of the waste water and fine minerals (Smith et al., 2013). Although

it is anticipated that the chimneys will reform at actively venting areas, the time that it will take for the recovery of the habitat depends on the local hydrothermal activity. Recovery from deep – sea mining extraction operations will depend upon the species mix and vary between sites. For hydrothermal vent fauna, recolonization by the biomass-dominant species after a major disturbance could happen in just a few years at active venting sites (Van Dover, 2010). However, this is not the case for all vent ecosystems and we lack enough information from most vents to predict their recovery following mining. In addition, at inactive sulphide mounds, chimney structures will not grow back, and any impact to the hard substrata will be long term. Visual recovery could, according to Van Dover, take a decade or more (Van Dover, 2010).

Concerning environmental management responsible objectives involve balancing resource use with maintaining deep-ocean ecosystem biodiversity. Management should therefore include consideration of any functional linkages between the ecosystem and the subsurface biosphere, the water column, the atmosphere, and the coasts, as well as the full range of goods and services that the ecosystem provides. A description of the existing environment will be needed, where effective monitoring of any impact will be dependent upon detailed baseline studies that establish a benchmark prior to seabed mineral activities (Smith et al., 2013).

A mentioned above, inactive sites remain to a large extend unexplored and, as a consequence, invertebrate taxa colonizing inactive sulphide mounds that might be targeted by mining are much more poorly characterized than those of active hydrothermal vents. Issues that needs to be explored are e.g. biodiversity, rates of recruitment, succession, or population structure of organisms colonizing inactive sulphides in any ocean basin (Van Dover, 2010). Inactive sites could also include areas classified as vulnerable marine ecosystems (VME) by the International Council for the Exploration of the Sea (ICES, 2016) and OSPAR (Hogg et al., 2010), and would need to be treated accordingly (Levin et al., 2010). There is not even done enough research of these sites to be sure if there in fact is a specialised fauna adapted to the particular geochemical and microbial conditions of weathering sulphide mineral substrata (Van Dover, 2010). This is also true for inactive sites in the Norwegian waters, and as mining activity will most likely mainly be confined to inactive sites, this lack of knowledge calls for new and comprehensive surveys in inactive areas (Rapp, 2015).

1.6. The MarMine project

MarMine (BIA project co-funded by NFR and industrial partners (https://www.ntnu.edu/igb/marmine) is an important part of NTNU's focus on marine mineral resources, and the project is established to estimate the undiscovered mineral resource potential on the extended Norwegian continental shelf, focusing on SMS deposits along the AMOR and evaluate the potential environmental impacts of mining operations. The ridge is largely unmapped with high resolution bathymetry and preliminary indications of resource potential has considerable uncertainty. One of the goals of this project is to reduce the uncertainty and update the estimates for degree of mineralization by exploring the seabed and taking samples. The project as a whole considers multiple challenges related to subsea mineral deposits such as exploration, extraction, processing, metallurgy, infrastructure, economic, marketing, legal, environmental, social and governmental factors. The MarMine cruise attempts to address the challenge of exploration directly, and others indirectly by providing crucial samples for further research. The project intends to do both geological and biological sampling and analyses (Sture, 2016).

As this introduction has stated, the need for exploration and mapping of inactive vent fauna is dire. To better understand the ecosystems there and how they might be affected by anthropogenic disturbance, both research and commercial, is crucial to make the right decisions regarding the future of such commercially interesting areas. This is what this thesis aims to do, contribute to the understanding of benthic megafauna communities of geologically inactive vent sites.

1.7. Main goal

Describe, for the first time, the benthic megafauna communities of the geologically inactive site of Mohn's Treasure (AMOR) by analysing photo transects taken with a remotely operated vehicle.

1.8. Sub goals

1. Identify the megafauna species observed in the photo transects to the lowest taxonomic level possible.
2. Quantify the densities of the different species/taxa observed at Mohn's Treasure through quantification of photo transects.
3. Compute biodiversity indices for the Mohn's Treasure site.

2. Materials and methods

2.1. Study location

All sampling for this thesis was gathered on board the multipurpose subsea vessel *CSV Polar King* during a research cruise in the framework of the MARMINE project in the summer of 2016. The cruise was conducted between the 15th of August and 5th of September. The area examined during the cruise were the active vent site of Loki's Castle, the inactive site of Mohn's Treasure, as

Fig. 3. Areas of operation. Shows the 4 different locations examined during the MarMine cruise of the summer 2016. The inactive site of Mohn's Treasure is located 30 km south-west of the black smoker vent field of Loki's Castle, discovered by UiB in 2008. From Sture, 2016.

well as two areas of exploration (Fig. 3), all situated on the AMOR.

The area studied for this thesis was the geologically inactive site of Mohn's Treasure at 73°44'N 07°27'E. As previously mentioned, Mohn's Treasure is situated at the edge of an inner rift wall 30 km south-west of the black smokers of Loki's Castle (Fig. 3).

For the purpose of this thesis, the area was divided into 3 distinct sampling sites, based on differences in the available bathymetric data, substrate and steepness gradient. The reason for this dividing was to get the best representation of the Mohn's Treasure megafauna with the limited sampling resources available.

Site 1 (Fig. 4) makes up the deepest parts of Mohn's Treasure, being a gentle slope at approx. 2810 m. The site consists of mainly soft sediment with some rocks of various sizes spread around. The slope, on which *Site 1* is located, continues to increase in depth beyond 3000m (Fig. 4).

Site 2 (Fig. 4) is located at approx. 2740m depth and is located on what resembles a plateau regarding steepness and topography. *Site 2* is quite similar to *Site 1*, consisting of mainly

13

soft sediment, with some assemblages of rocks and boulders. The lower part of *Site 2* is marked by a small ridge of hard substrate.

     Site 3 (Fig. 4) differs more from the other two sites in depth, located at approx. 2390m depth. It consists of mainly soft sediment but often with coarser sediments and areas covered with small rocks. The steepness gradient is greater than for the other sites, and at the upper part ends with a sedimentary slope.
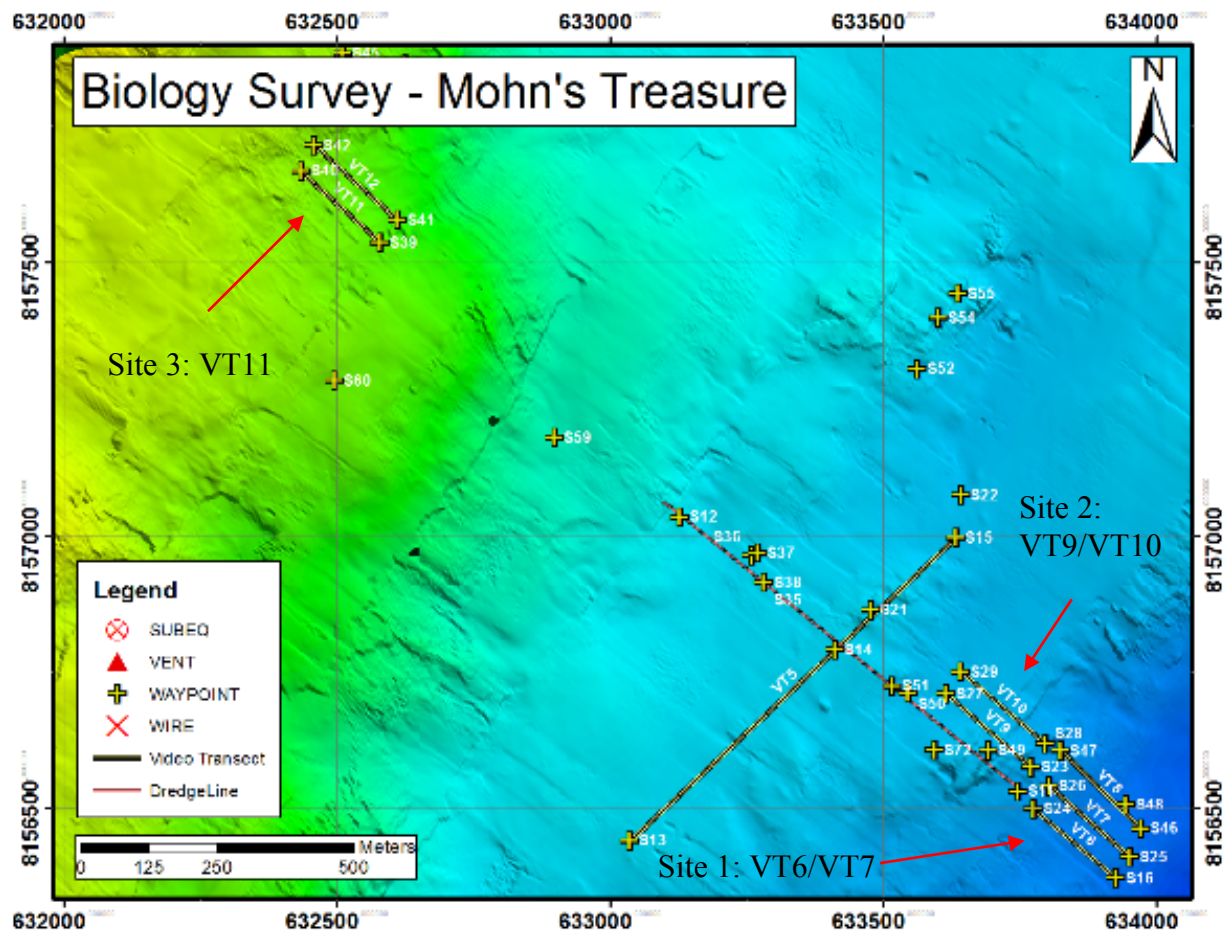
Fig. 4. Inactive site of Mohn's Treasure, Mohn's Ridge. Showing the biological surveys done during the MarMine cruise 2016. Site 1 consists of VT6 – VT8, and can be found in the lower right corner of the image. Site 2 consists of VT9 – VT10, and is sees between site 1 and VT5 (long transect perpendicular to the other transects). Site 3 consists of VT11 – VT12, and can be found in the upper left corner. Modified from Sture, 2016.

2.2. Equipment specifics

CSV Polar King was equipped with two Triton Work class Remotely operated vehicles (ROV), named XLR 02 and XLX 57 (Appendix, A1) with Tether Management System (TMS) (Sture, 2016). Only the XLR was used for video-/photo transects (VT/PT). The ROVs were equipped with low light navigation cameras *Kongsberg OE13-124* (XLR 02), *Kongsberg 15-110c*, (XLX 57) and CCD colour camera *Kongsberg 14-366* for still photos (Appendix, A2) (Sture, 2016).

The ROVs were equipped with two green lasers (532nm), projecting two parallel laser lines on the seafloor with a distance of 10 cm (Fig. 5). These lines can be used to calibrate the camera field of view.
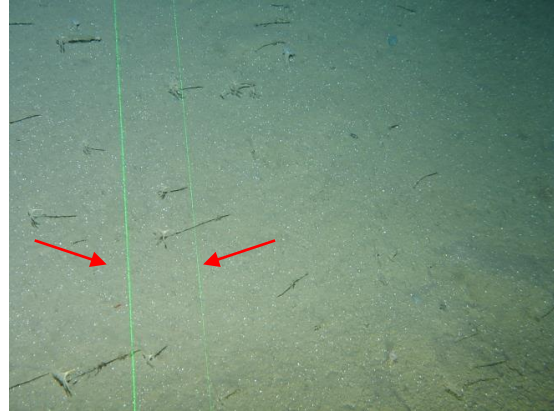
Fig. 5. Photo from Mohn's Treasure, Site 1, showing the two green laser lines (distance 10 cm) (arrows) used to calculate the photo square size. In the photo can be seen the crinoid Bathycrinus Carpenteri

2.3. Video-/photo transects (VT/PT)

The VTs/PTs were conducted flying the ROV at a specific height (1 m) above the sea floor and at a constant speed of 0.4 knots (0.2 ms^{-1}). Due to variations in environmental factors such as topography and currents, the distance above seafloor and speed slightly varied during the transects.

All dives were still being recorded with the low light navigation video cameras *Kongsberg OE13-124*, but during the video transects, we also used the CCD colour photo camera *Kongsberg 14-366*. Although the original plan for this project was to analyse video transects, the video camera on the ROV was not high resolution, making the analyses of the images for faunal identification difficult. We thus decided to take regular photos during all video transects and use these higher resolution images for the analyse.

The still photos (*Kongsberg 14-366*) were taken at an interval of approx. 15 seconds apart. The reason for this interval was that the strobe needed time to recharge between shots. Due to factors on board, the interval between the pictures varies up to max 60 seconds. During

A total of 8 transects were conducted at Mohn's Treasure (Table 1), with one transect of 800 m (VT5) perpendicular to the other shorter transects. Three replicates (VT6 – VT8) of

200 m at *Site 1*, 2 replicates (VT9 – VT10) of 200 m at *Site 2* and 2 replicates (VT11 – VT12) of 200 m at *Site 3*.

Table 1 Overview of dive metadata conducted during the MarMine cruise August – September 2016 on board the CSV Polar King. The data used for this thesis is gathered from VT6, VT7, VT9, VT10 and VT11, conducted between the 23th and 25th of August, 2016.

Transect	ROV dive nr.	Date	Start site	End site	Length (m)	Depth (m)	Location
VT5	ROV8	24.08.2016	S13	S15	800	2700	Mohn's Treasure
VT6	ROV8	24.08.2016	S16	S24	200	2810	Mohn's Treasure
VT7	ROV8	25.08.2016	S25	S26	200	2810	Mohn's Treasure
VT8	ROV10	26.08.2016	S46	S47	200	2810	Mohn's Treasure
VT9	ROV5	23.08.2016	S23	S27	200	2745	Mohn's Treasure
VT10	ROV5	23.08.2016	S28	S29	200	2750	Mohn's Treasure
VT11	ROV9	25.08.2016	S39	S40	200	2385	Mohn's Treasure
VT12	ROV9	25.08.2016	S41	S42	200	2385	Mohn's Treasure

Estimating the square size of the seabed covered from photographs or video is an important issue in seafloor studies (Dias et al., 2015). The movement of platforms such as submersibles, towed vehicles or, in this case, remotely operated vehicles, makes this task complex to achieve (Dias et al., 2015). The XLR 02 was equipped with two green laser lines (Fig. 5) to help calculate the square size of each photo. Because of the optical distortion of the laser lines on particles in the water during the transects, photos with laser lines were taken before some of the transects. The square size of each photo was calculated using the approach in A3 (Appendix). The method is based on knowing distance above seafloor, incline angle of the seafloor, camera angle, image width/height and camera vertical/horizontal field of view (FOV). A challenge with the ROVs used, being specialised to industrial purposes mainly instead of research, was that camera data such as camera angle and FOV was not logged. This, combined with a lack of sufficiently detailed bathymetry, has led to several assumptions being made to be able to estimate the square size of the photos. The assumptions have been made in cooperation with Stein Nornes Melvær and Øystein Sture, PhD student at Department of Marine Technology, NTNU, that participated in the cruise, specialised in underwater photography. Since most parts of the transects are relatively flat, the incline angle of the seafloor has been set to 0°. Based on the setting request for the camera prior to each dive, the camera angle has been set to 50°. Based on the photos with laser lines, the camera FOV was calculated to 17°x12,75°.

2.4. Image selection and analysis

The number of photos taken in each transect varied between 68 and 108 (Table 2). Because of the difference in ROV speed and the frequency of the still photos, some photos overlapped regarding seabed covered. These photos were excluded from the dataset, to avoid spatial overlap and replication of features. This made up the datasets of between 52 photos (VT10) and 76 photos (VT6) in each transect (Table 2). According to Taylor et al., (2017) who have utilized photographic transects using towed vehicles to conduct time-series studies extending longer than a decade at the HAUSGARTEN observatory in the Fram Strait, a number of 80 images per transect is sufficient to capture the taxon inventory. In their study species/taxa accumulation curves for each transect headed towards a plateau after 15 – 25 images (Taylor et al., 2017).

At the second last photo transect (VT11) the memory card of the CCD camera was filled during the transect, and the last transects were documented using an AVT 1380C camera to collect 2D still images. These photos can be used to make a photo mosaic of the transect. However, the images were quite different regarding field of view, light sensitivity and colours, so they were not included in the dataset. This has led to *Site 3* being represented with data from VT11 only. Due to this, and other various factors, the data for this thesis is based on VT6 and VT7 from *Site 1*, VT9 and VT10 from *Site 2* and VT11 from *Site 3* (Table 2).

Table 2 List of photo transects used for this thesis. VT6/VT7 makes up *Site 1*, VT9/VT10 makes up *Site 2*, while *Site 3* comprises of only VT11. Included is also basic environmental factors logged during the ROV dives (depth/temp).

Transect	Site	Depth (m)	Depth variation (m)	Temperature (ºC)	No. images taken (no. analysed)
VT6	1	2826 – 2796	30	-0.717	108 (**76**)
VT7	1	2823 - 2789	34	-0.715	94 (**69**)
VT9	2	2757 - 2727	30	-0.719	99 (**63**)
VT10	2	2769 - 2729	40	-0.718	68 (**52**)
VT11	3	2390 - 2379	11	-0.744	102 (**62**)
Overall	1 – 3	2826 - 2379	447	-0.723*	471 (**322**)

*mean value

Each image was labelled twice, to even out learning effects. All analyses were conducted in a shaded room to reduce external glare, and the same computer was used in all analyses to remove variation brought about by varying resolution.

The transects were analysed both qualitatively and quantitatively. All species observed have been identified to the lowest taxonomic level possible. The identification of species has been done partly by use of literature (Clark, 1970; Madsen et al., 1994), but the main

contribution to species identification has been in cooperation with Hans Tore Rapp, at the Department of Biology, UiB, wo has first-hand experience from the region.

Abundances of different species have been quantified for each transect and the densities of different species (number of ind. m^{-2}) have been calculated for each transect, and the mean and standard deviation densities per site has been calculated. Since *Site 3* consisted only of data from VT11, mean densities and standard deviation could not be conducted.

Shannon-Weaver diversity and Pielou's evenness were computed for each transect/site to compare the indices between the different parts of Mohn's Treasure.

3. Results

The present study is the first to look at benthic megafauna communities at the geologically inactive area of Mohn's Treasure, AMOR. In total 322 photos were analysed, comprising an area of 486 m^2 (Table 3) with mean areas per photo of 1.51 ± 0.41 m^2 ($\pm$ SD).

Table 3. Area covered by photo transects, mean and standard deviation (SD) values. *Site 1* consists of VT6 and VT7, *Site 2* of VT9 and VT10, whilst *Site 3* consists only of, and is identical with, VT11. Overall data shows total no. of photos analysed and total area of Mohn's Treasure that has been sampled.

Dataset	No. of photos	Area covered (m^2)	Mean area per image (m^2)	±SD
VT6	76	104	1.4	0.24
VT7	69	125	1.8	0.75
VT9	63	96	1.5	$4.44*10^{-16}$
VT10	52	75	1.5	0.12
VT11	62	85	1.4	0.15
Site 1	145	239	1.6	0.59
Site 2	115	172	1.5	0.09
Site 3	62	85	1.4	0.15
Overall	322	486	1.5	0.41

3.1. Taxonomic analysis

A total of 43 taxa and morphotypes were recorded across all transects (Table 4), with 15 being identified to species level: (Fig. 6), five organisms identified to genus level (Fig. 7), four taxa identified to family level (Fig. 7), and two crustaceans identified to order level (Fig. 7). The remaining 17 organisms that could only be identified to class level includes two species of glass sponges (Hexactinellida spp.), two morphotypes of bristle worms (Polychaeta), and 11 unidentified morphotypes of Demospongiae (Fig. 8). The unidentified Demospongiaes were given artificial names of conventional reasons and sorted and counted as respectively "Demospongiae morphotypes 1 – 7" and "Encrusting demospongiae morphotypes 1 – 7" (Fig. 8. In addition to these taxa/morphotypes, there were several interesting observations in the photo transects that could not be identified to even class/phylum due to low image resolution. A photo collage of these unidentified objects can be found in B2 in the appendix.

Table 4. Number of species/taxa in each photo transect (VT6 – 11), per site (*Site 1 – 3*) and overall number of specimens.

Transect	VT6	VT7	VT9	VT10	VT11	Site 1	Site 2	Site 3	Overall
No. of species/morphotypes	27	27	35	29	32	31	36	32	43
No. of specimens	2567	4333	2838	2531	2420	6900	5369	2650	14919
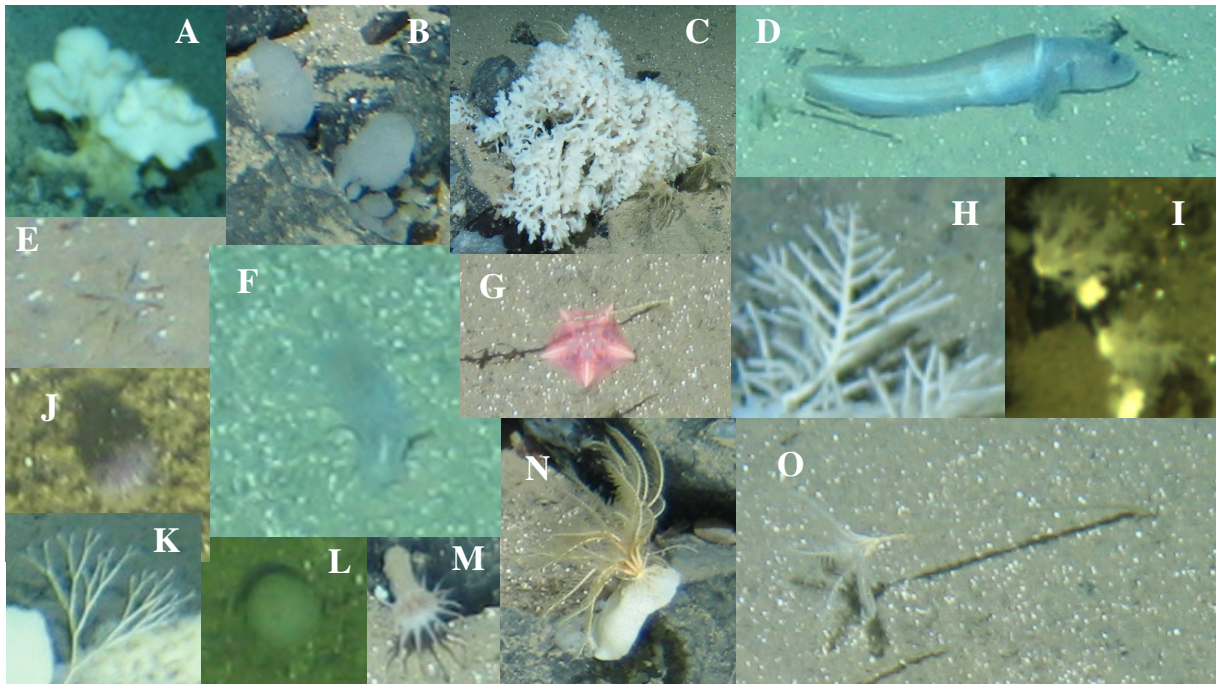
Fig. 6. Organisms identified to species level, Mohn's Treasure. (A) *Caulophacus arcticus*, (B) *Brattegardia* sp. *nov* (C) *Lyssodendoryx complicate*, (D) *Lycodes frigidus*, (E) *Ascorhynchus abyssi*, (F) *Kolga hyaline*, (G) *Hymenaster pellucidus*, (H) *Cladorhiza gelida*, (I) *Gersemia fruticosa*, (J) *Pourtalesia jeffreysi*, (K) *Asbestoplumea furcate*, (L) *Thenea abyssorum*, (M) *Bathyphellida margaritacea*, (N) *Poliometra prolixa*, (O) *Bathycrinus carpenterii*.
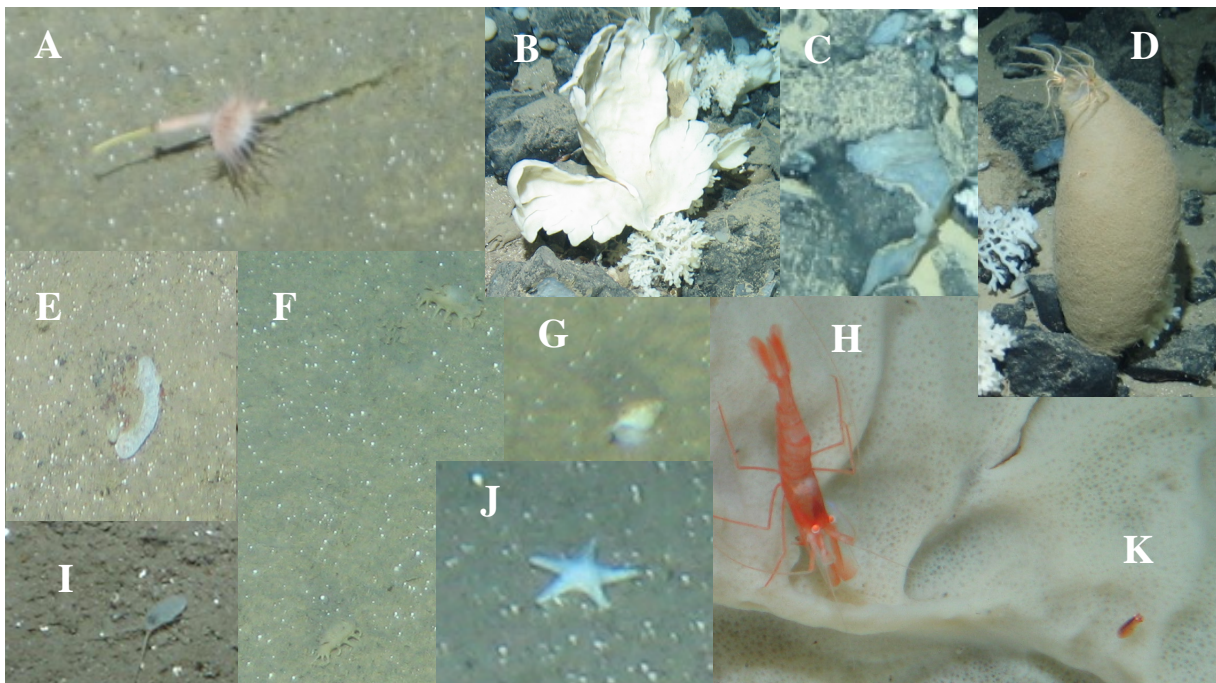
Fig. 7. Organisms identified to genus/family/order level, Mohn's Treasure. (A) *Amphianthus* sp. (B) Axinellidae indet. (C) *Hymedesmia* sp. (blue encrusting sponge) (D) *Asconema* sp. (E) Didemnidae indet. (F) *Elpidia* sp. (G) Buccinidae indet. (H) *Bythocaris* sp. (I) Isopoda indet. (J) Poraniidae indet. (K) Amphipoda indet.
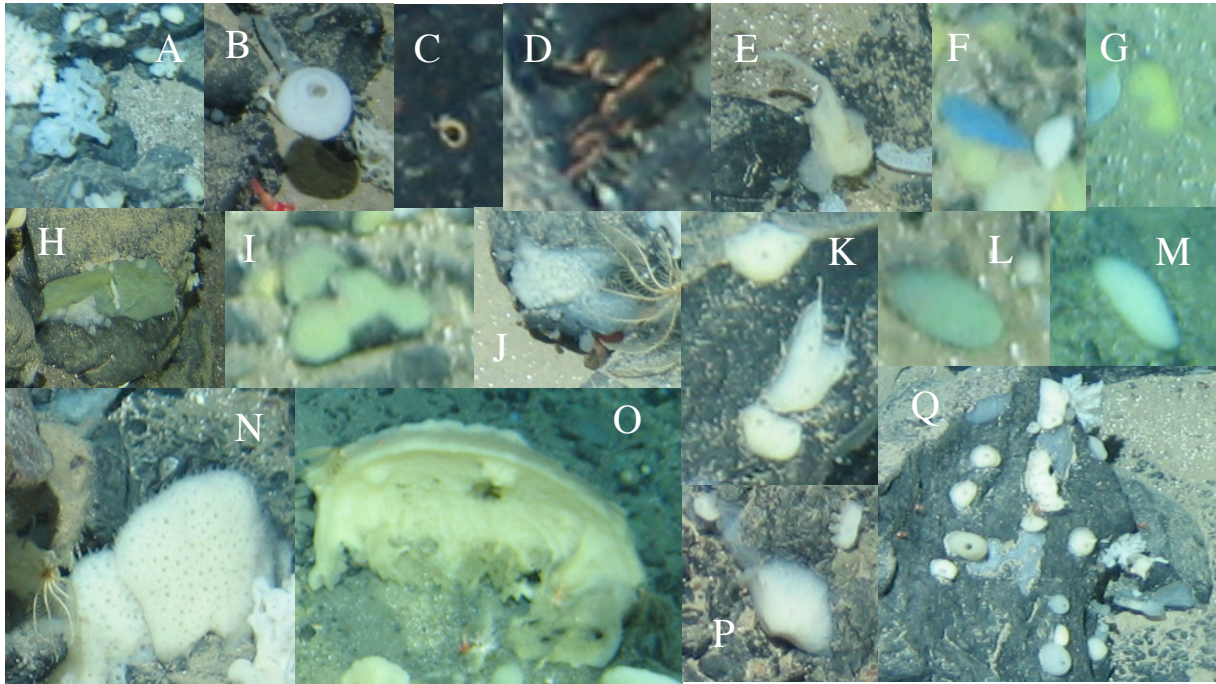
Fig. 8. Organisms that could not be identified to order level or lower, Mohn's Treasure. They have been classified and ordered for counting based on differences in morphotypes characteristics (pheotypes better word?). (A) Hexactinnelida morphotype 1, (B) Hexactinnelida morphotype 2, (C) Polychaeta morphotype 1, (D) Polychaeta morphotype 2, (E) Demospongiae morphotype 5, (F) Encrusting sponge morphotype 1, (G) Encrusting sponge morphotype 7, (H) Encrusting sponge morphotype 3, (I) Encrusting sponge morphotype 4, (J) Encrusting sponge morphotype 5, (K) Encrusting sponge morphotype 6, (L) Demospongiae morphotype 6, (M) Demospongiae morphotype 4, (N) Demospongiae morphotype 1, (O) Demospongiae morphotype 2, (P) Demospongiae morphotype 7, (Q) Demospongiae morphotype 3. Demospongiae morphotypes 3 consists of white/beige/gray small, round sponges with one or more holes.

Species accumulation curves (Fig. 9) showed that a sample of approx. 35 - 45 photos per transect will most likely be sufficient to capture the taxon inventory as the curves for each transect headed towards a plateau. One exception was VT6, which lay at a plateau from photo no. 29 to photo no. 49. At photo no. 49 the transect encountered a shift in habitat from sediment to medium sized boulders, presenting 6 new taxa before stabilizing again from photo 52 and throughout the rest of the transect. (76 photos, Table 3, Fig 9). The graph shows that number of species in the first photograph of each transect consisted of between 6 and 11 different species/taxa.
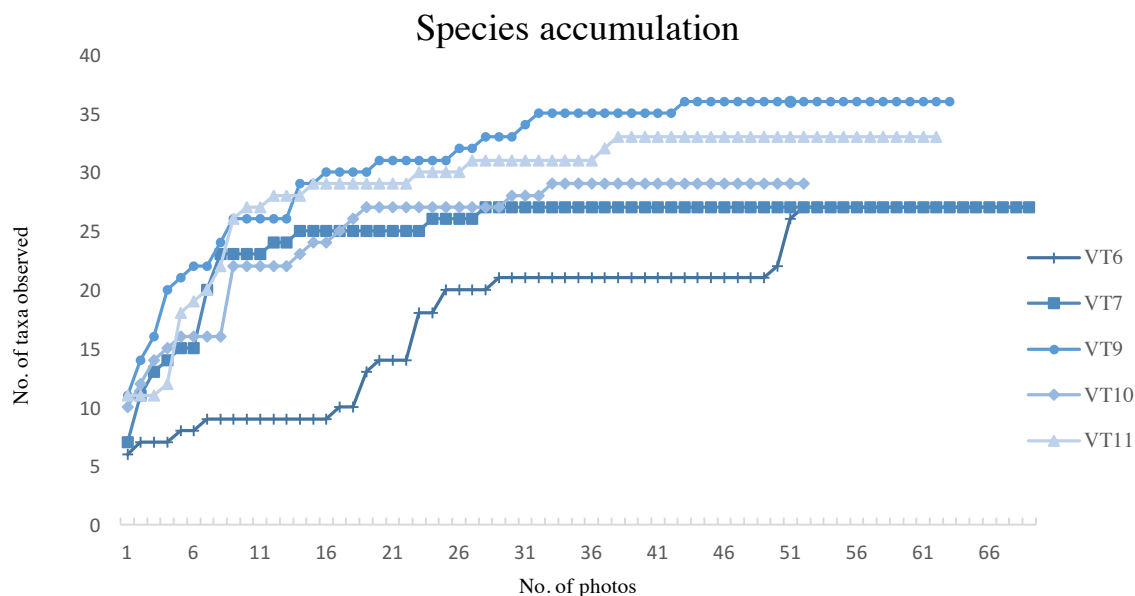
Fig. 9. Species accumulation curves for the different photo transects (VT) taken at Mohn's Treasure. The x-axis shows no. of photos, while y-axis shows the accumulation of new taxa, as new taxa are encountered going from the start of each transect (photo no. 1) to the end. Shows how VT6 encountered new species/taxa at photo no. 49, after being stable since photo no. 29.

3.2. Habitat features and overall faunal community observations

The 3 sites investigated at Mohn's Treasure are dominated by soft sediment substrata (silt, clay and sand) (Fig. 10), with various degrees of pebbles, small rocks and areas of bigger boulders (Fig. 11).

Site 1 in the lower slope (2810 m depth) was to the largest extend dominated by soft sediment substrata (Fig. 10), with one small region of spread medium sized rocks and one appearance of big boulders (Fig. 11), making up approx. 6% hard substrata (Table 5) for the area.

Site 2 on what was called the plateau (2740 m depth), was also covered by fine sediment, but included a higher degree of hard substrata than *Site 1*, (approx. 22%, Table 5), in the form of medium sized rocks and medium sized boulders at the lower part of the area (Fig. 12).

Site 3 on the upper slope (2390 m depth) had the highest occurrence of hard substrata (approx. 35%, Table 5) in the form of rocks of medium to small size (Fig. 13). The sediment seemed coarser in some places, compared to the deeper sites.

Table 5   Estimates of occurrence of hard substrata in the dataset.

Transect	Site 1	Site 2	Site 3
Total no. of photos	202	167	102
No. of photos with hard substrata	12	37	36
% of photos with hard substrata	5.9	22.2	35.3
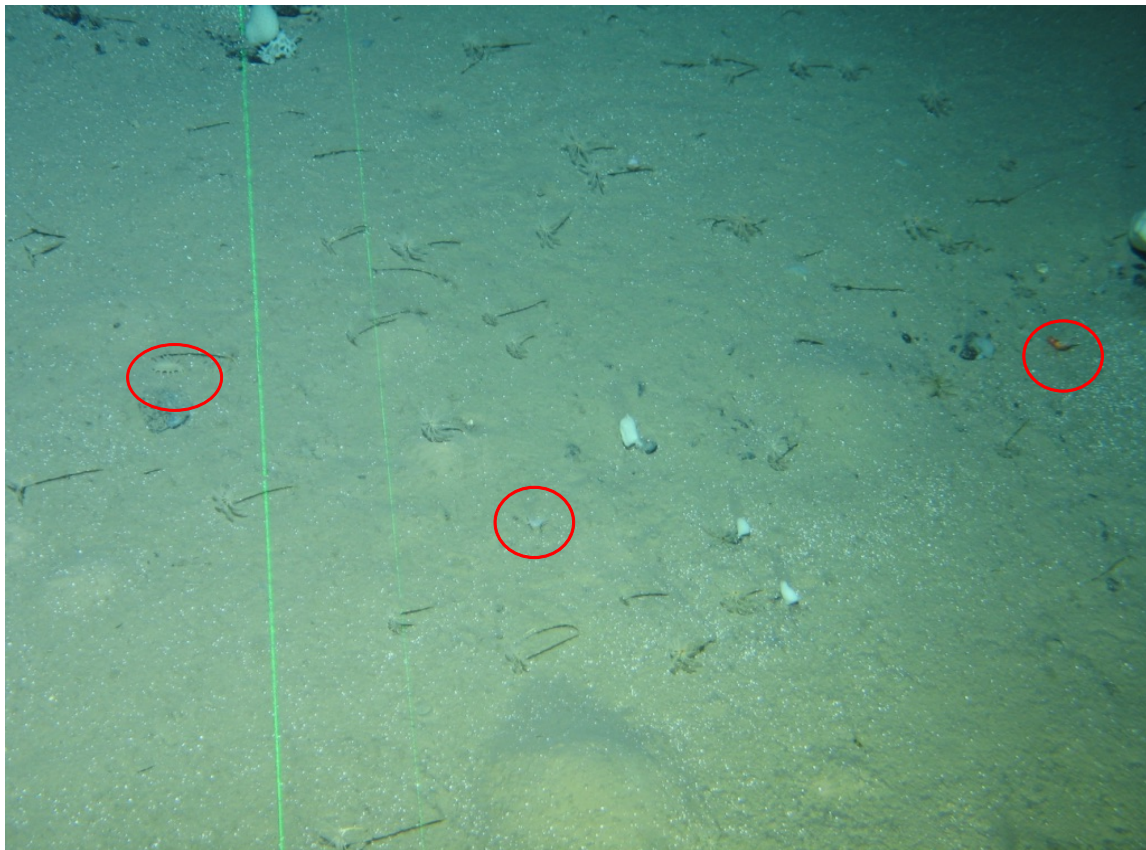
Fig. 10. VT6 and VT7 (*Site 1*) is mainly dominated by soft substrata, which again is dominated by the suspension feeding stalked crinoid *Bathycrinus carpenterii*. To the left of the lasers can be spotted the holothurian *Elpidia* sp. (left red circle), In the middle of the photo can be spotted the cnidarian *Bathyphellida margaritacea* (middle red circle) and on the far right in the middle a the crustecean *Bythocaris* sp. (right red circle). The distance between the lasers are 10 cm.
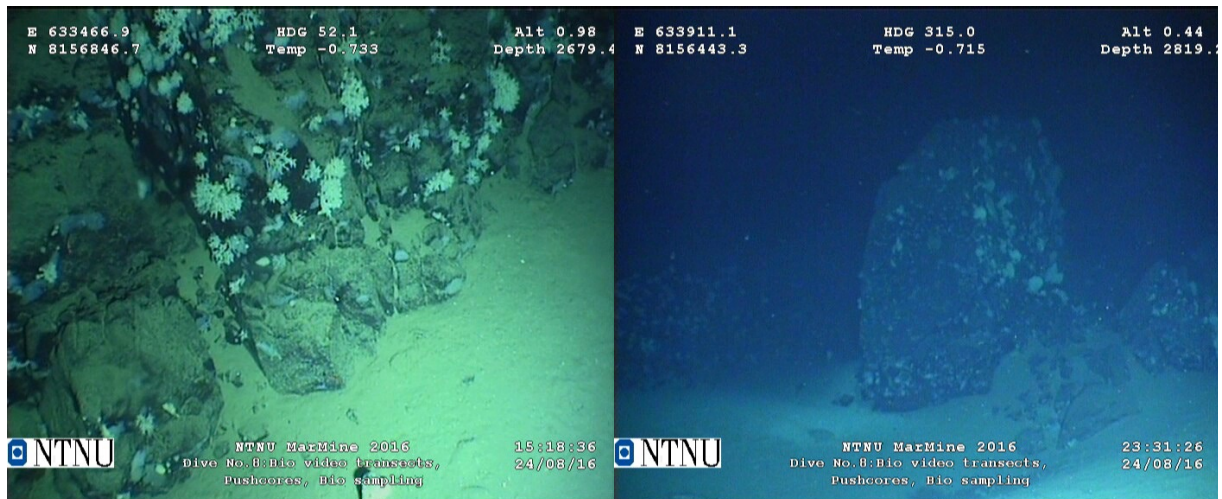
Fig. 11. Screenshots taken from the ROV low light navigation camera "Kongsberg OE13-124" conducted during ROV dives on board CSV Polar King. The screengrabs show basic environmental data; temperature and depth, in addition to time/date, distance above seafloor (Alt) and coordinates. The left photo was taken from VT5, whilst the right photo shows a large boulder inhabited by sponges during VT7.

Fig. 12. Photo from VT9, showing a typical area of hard substrate composed of small rocks. In the middle of the photo can be seen a glass sponge of the genus *Asconema sp* (brown), and an unidentified glass sponge (white) with a *Bythocaris* (red) next to it. In the upper right corner can be spotted the sponge *Caulophacus arcticus*. The coral-like white sponge seen all over the photograph is the demospongiae *Lyssodendoryx compliata*.
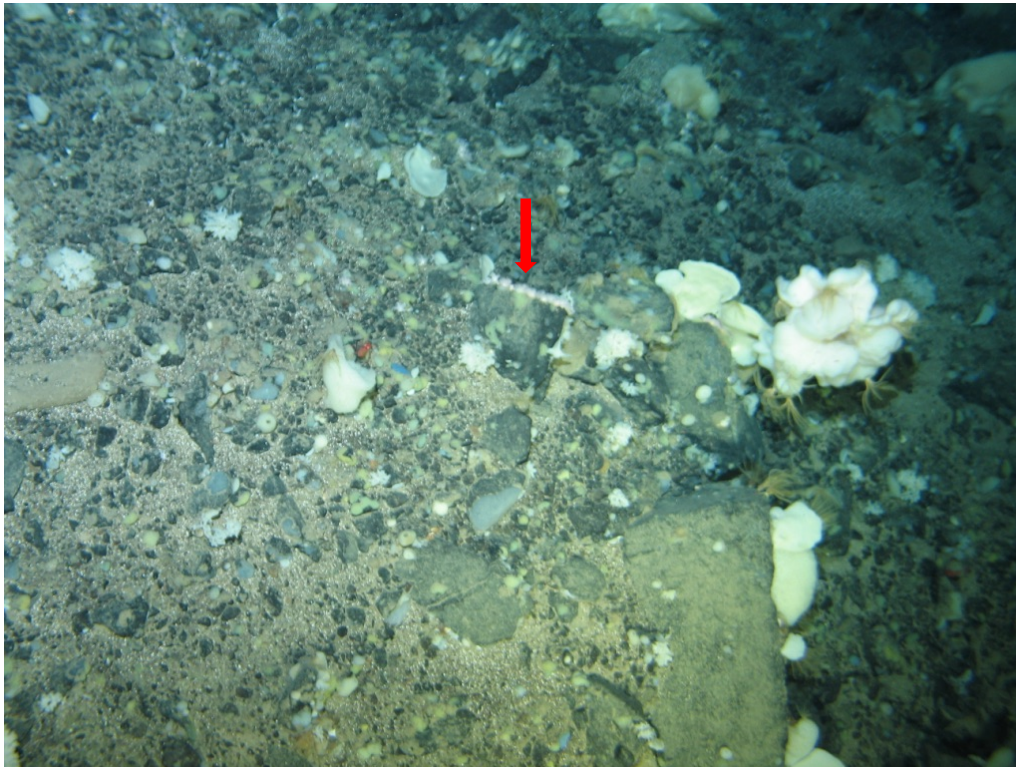
Fig. 13. Photo from VT11, showing how the substrate often was made up of a mix of small rocks/pebble, and some medium sized rock. The white fans are sponges of the order Axinellidae. The *Caulophacus arcticus* seen on the right side is inhabited by several crinoids of the species *Poliometra prolixa*. The blue/grey sponges seen as a coat on hard substratum belong the genus *Hymedesmia*, and the arrow shows a colony of the octocoralida *Gersemia fruticosa*. VT11 is inhabited by large amounts of small sponges (white, gray, beige, green, yellow, blue) that cannot be identified from the available photographs.

The soft sediment was mainly inhabited by stalked crinoids and mobile fauna such as holothurians, asteroids and crusteceans (Fig. 10). *Site 1* was characterisez by the presence of vast fields of the stalked crinoid *Bathycrinus carpenterii* (Fig. 10). When there is a change in substrate type, from sediment to rock, there is also an immediate cange in species occurrences. The rocks and boulders were colonised by abundant sponges of different species, crinoids and crusteceans (Fig. 12). Abundance plots for VT6 - VT11 can be found in appendix (B2-B6).

The studied benthic megafaunal communities of Mohn's Treasure comprise organisms represented by 8 different phyla (Fig. 14) and at least 43 different species (Table 4). In relation to the number of species/morphotypes per phylum, the Porifera is by far the most diverse group with 25 different morphotypes, followed by the Echinodermata with 7 different taxa (Fig. 15). These two groups (echinoderms and sponges) are the most abundant in terms of individuals, with 50% and 37% respectively (Fig. 14). The dominating species at Mohn's Treasure is the stalked crinoid *Bathycrinus carpenterii*, alone making up 47% of the counted organisms (Fig. 16) with a total abundance of 6960 (Appendix, B7). The sponges *Lyssodendoryx complicata* and *Hymedesmia* sp. each represents 8% of the recorded abundances (Fig. 16), the former with 1119 observed individuals, and the latter 1120 observed individuals (Appendix, Table 3).

Relative abundance of phyla observed, Mohn's Treasure

- Porifera
- Cnidaria
- Mollusca
- Annelida
- Pycnogonida
- Crustacea
- Echinodermata
- Chordata

1 %

37 %

50 %

9 %

1 %

1 %

1 %

0 %
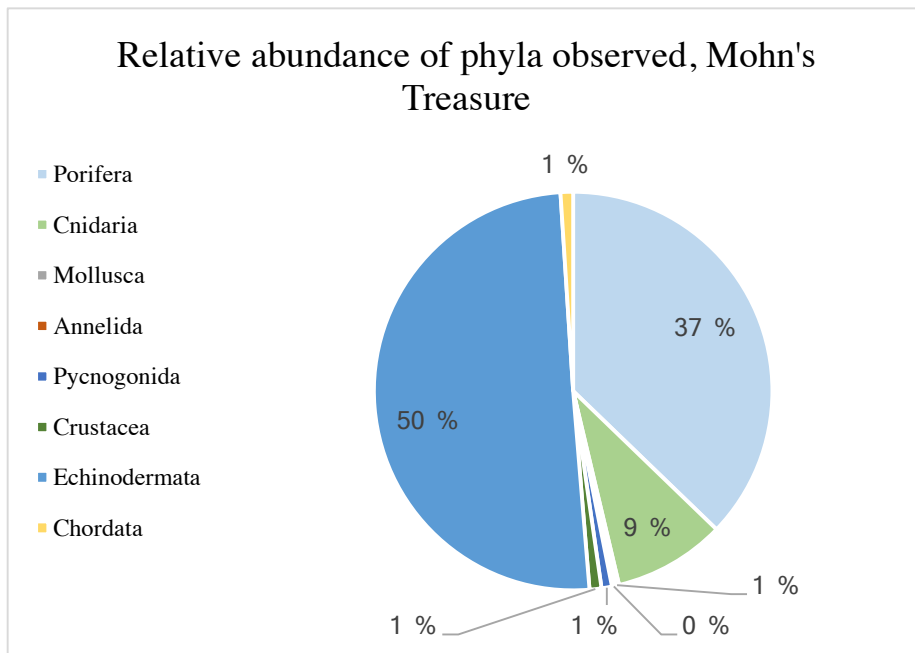
Fig. 14. Pie chart of relative megafaunal abundances divided into phyla. The chart shows differences in abundances, showing a clear dominance of echinoderms and sponges, followed by cnidarians.

3.3. Trophic traits of the Mohn's Treasure megafauna

The most common trophic feeding type at Mohn's Treasure is suspension feeding, followed by predators/scavengers and last deposit feeders (Fig. 15). The phylum Porifera (sponges) constitute the biggest number of suspension feeders, together with sessile Echinodermata, such as the crinoids *Bathycrinus carpenterii* and *Poliometra prolixa*.

Taxon	Phy	FT	VT6	VT7	VT9	VT10	VT11
Caulophacus arcticus	P	SF					
Asconema sp.	P	SF					
Hexactinellida sp. 1	P	SF					
Hexactinellida sp. 2	P	SF					
Brattegardia sp. nov	P	SF					
Lyssodendoryx complicata	P	SF					
Asbestopluma furcata	P	SF					
Cladorhiza gelida	P	SF					
Hymedesmia sp.	P	SF					
Axinellidae sp.	P	SF					
Thenea abyssorum	P	SF					
Encrusing sponge morphotype 1	P	SF					
Encrusing sponge morphotype 2	P	SF					
Encrusing sponge morphotype 3	P	SF					
Encrusing sponge morphotype 4	P	SF					
Encrusing sponge morphotype 5	P	SF					
Encrusing sponge morphotype 6	P	SF					
Encrusing sponge morphotype 7	P	SF					
Demospongiae morphotype 1	P	SF					
Demospongiae morphotype 2	P	SF					
Demospongiae morphotype 3	P	SF					
Demospongiae morphotype 4	P	SF					
Demospongiae morphotype 5	P	SF					
Demospongiae morphotype 6	P	SF					
Demospongiae morphotype 7	P	SF					
Gersemia fruticosa	Cn	SF					
Amphianthus sp.	Cn	SF					
Bathyphellida margaritacea	Cn	SF					
Buccinidae sp. 1	M	P/S					
Polychaeta sp. 1	A	n.d					
Polychaeta sp. 2	A	n.d					
Ascorhynchus abyssi	Py	P/S					
Bythocaris sp.	C	P/S					
Isopoda sp.	C	DF					
Amphipoda sp.	C	DF					
Bathycrinus carpenterii	E	SF					
Poliometra prolixa	E	SF					
Hymenaster pellucidus	E	P/S					
Poraniidae sp.	E	P/S					
Pourtalesia jeffreysi	E	DF					
Kolga hyalina	E	DF					
Elpidia sp.	E	DF					
Didemnidae sp.	Ch	SF?					
Lycodes frigidus	Ch	P/S					
Feeding group							
Predators/scavengers							
Suspension feeders							
Deposit feeders							
Overall densities							

Fig. 15. Heatmap Mohn's Treasure. Showing the relative abundance of each taxa/morphotype and trophic feeding type (FT). (Phy) Phymul: (P) Porifera, (Cn) Cnidaria, (A) Annelida, (M) Mollusca, (Py) Pycnogonida, (C) Crustacea, (E) Echinodermata, (Ch) CHordata (see Table 6 for abundance data). (FT) Feeding type: (SF) suspension feeder, (P/S) predator/scavenger, (DF) deposit feeder, (n. d.) not defined.

Relative abundance intensity
Highest
Lowest
Absent

27
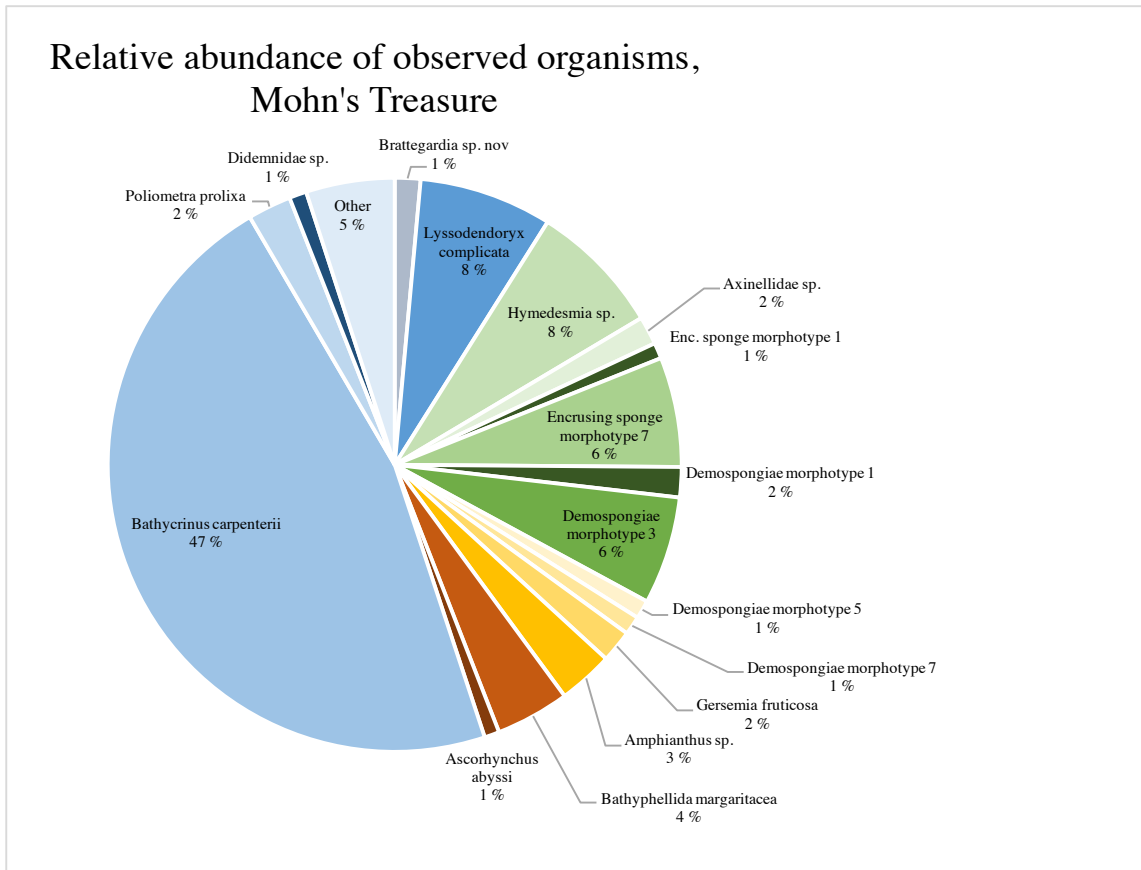
Fig. 16. Pie chart of relative abundances of observed megafaunal organisms for Mohn's Treasure, AMOR. The slice "Other" is compriced of: *Caulophacus arcticus, Asconema* sp. Haxactinnellida indet. 1 and 2, *Asbestopluma furcata, Cladorhiza gelida, Thenea abyssorum*, Encrusting sponge morphotype 3 – 6, Demospongiae morphotype 2, 4 and 6, *Buccinidae* sp. Polychaeta indet.1 and 2, *Bythocaris* sp., Isopoda indet., Amphipoda indet., *Hymenaster pellucidus*, Poranoiidae indet., *Pourtalesia jeffreysi, Kolga hyalina, Elpidia* sp. *and Lycodes frigidus*. These taxa/morphotypes have been sorted under "Other" based on their total abundances being under 100 throughout all the VTs.

3.4. Community structure and diversity

3.4.1. Mean densities and diversity indices per site

Site 1 (VT6/VT7) had a species richness of 31 different taxa/morphotypes (Table 4, Fig. 17) and a total no. of specimens of 6900 (Appendix, B7). The mean density for *Site 1* was 29.563 ± 4.990 ind. m^{-2}, whilst the mean species density for all taxa was 1.095 ± 4.431 ind. m^{-2} (Table 6). Shannon – Weaver index *H* was 1.771 and Pielou's evenness *J* was 0.515 (Table 7). The areas with sediment is dominated by the stalked crinoid *Bathycrinus carpenterii*, with an abundance over 15 - 20 times higher than the next species for *Site 1* (Fig. 15, Appendix, B7). The density of *Bathycrinus carpenterii* for *Site 1* is 22.970 ± 6.424 ind. m^{-2} (Table 6).

Site 2 (VT9/VT10) had a species richness of 36 different taxa/morphotypes (Table 4, Fig. 17) and a total no. of specimens of 5369 (Appendix, B7). The mean densitiy for *Site 2* was 31.688 ± 2.028 ind. m^{-2}, whilst the mean species density for all taxa was 0.990 ± 2.0561 ind. m^{-2} (Table 6). Shannon – Weaver index *H* was 3.046 and Pielou's evenness *J* was 0.850 (Table

7). *Site 2* was also dominated by *Bythocaris carpenterii* (8.229 ± 7.207 ind. m^{-2}) (Table 6), but also had high densities of the demospongiaes *Lyssodendoryx complicate* (5.181 ± 1.622 ind. m^{-2}), *Hymedesmia* sp. (4.179 ± 0.130 ind. m^{-2}), Demospongiae morphotypes 3 (3.189 ± 0.556 ind. m^{-2}) and the cnidarian *Bathyphellida margaritacea* (2.643 ± 1.328 ind. m^{-2}), found attached to small rocks or buried in the sediment (Table 6).

Site 3 consists of only VT11, and therefore lacks the statistical analysis as standard deviation and variance. *Site 3* had a species richness of 32 different taxa/morphotypes (Table 4, Fig. 17) and a total no. of specimens of 2650 (Appendix, B7). Mean density for *Site 3* was 31.261 ind. m^{-2}, whilst the mean species density for all taxa was 0.977 ±1.979 ind. m^{-2} (Table 6). Shannon – Weaver index *H* was 2.420 and Pielou's evenness *J* was 0.698 (Table 7). The highest density recorded for *Site* 3 was for the encrusting sponge morphotypes 7 (10.676 ind. m^{-2}) (Table 6).
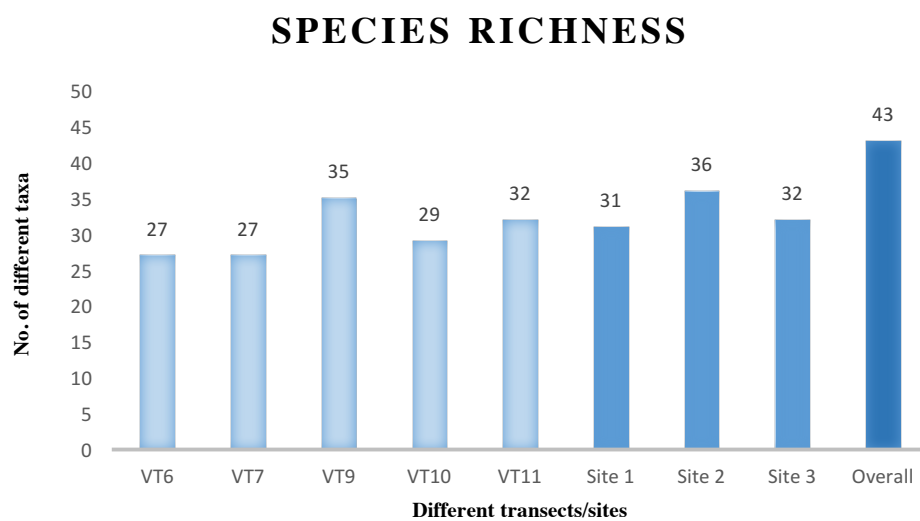
SPECIES RICHNESS

Fig. 17. Species/taxa richness. Shows each transect/site (x-axis) and its respective number of taxa observed (y-axis). VT9 is the single transect with the highest species richness of 35, and Site 2 is the site with most observed animal taxa. Overall species richness observed at Mohn's Treasure is 43 different species/taxa/morphotypes.

Table 6 Species/taxa densities per VT/Site. Showing mean density values for Site 1 (VT6+VT7) and Site 2 (VT9+VT10), including variance (Var.) and standard deviation (SD) where the data allows. Site 3 consists only of data from VT11, and therefore VT11 and Site 3 are identical. The frequency shows how many of the VTs each taxa have been represented in.

| Transect/site	VT6	VT7	VT9	VT10	VT11	Frequency %	Site 1 mean	Var.	±SD	Site 2 mean	Var.	±SD	Site 3
Porifera													
Caulophacus arcticus		0.008	0.042	0.027	0.071	80	0.004			0.034	$1.0*10^{-4}$	0.011	0.071I
Asconema sp.	0.029		0.115	0.120	0.012	80	0.013			0.117	$1.219*10^{-5}$	0.004	0.012
Hexactinellida sp. 1	0.019		0.052		0.024	60	0.009			0.029			0.024
Hexactinellida sp. 2			0.021	0.013	0.047	60				0.017	$2.868*10^{-5}$	0.005	0.047
Brattegardia sp.*nov*	0.642	0.080	0.668	0.825	0.153	100	0.361	0.158	0.397	0.747	0.012	0.111	0.153
Lyssodendoryx complicate	0.163	0.702	6.328	4.034	1.239	100	0.432	0.145	0.381	5.181	2.633	1.622	1.239
Asbestopluma furcate			0.021		0.047	40				0.012			0.047
Cladorhiza gelida					0.118	20							0.118
Hymedesmia sp.	0.402	1.236	4.271	4.087	2.442	100	0.819	0.348	0.590	4.179	0.017	0.130	2.442
Axinellidae indet.	0.278	0.183	0.710	0.493	0.944	100	0.213	0.004	0.067	0.601	0.024	0.154	0.944
Thenea abyssorum			0.042			20				0.023			
Encrusting sponge morphotype 1		0.016			1.545	40	0.009						
Encrusting sponge morphotype 3		0.016	0.063	0.120	0.047	80	0.009			0.091	0.002	0.040	0.047
Encrusting sponge morphotype 4					1.003	20							
Encrusting sponge morphotype 5	0.048	0.032	0.198	0.160	0.177	100	0.040	$1.0*10^{-4}$	0.011	0.179	0.001	0.027	0.177
Encrusting sponge morphotype 6			0.094	0.240	0.035	60				0.167	0.011	0.103	0.035
Encrusting sponge morphotype 7			0.167	0.027	0.676	60				0.097	0.010	0.099	10.,676
Demospongiae morphotype 1	0.211	0.112	1.316	0.466	0.672	100	0.161	0.005	0.070	0.891	0.361	0.601	0.672
Demospongiae morphotype 2			0.010		0.672	40				0.006			0.059
Demospongiae morphotype 3	0.622	1.101	3.582	2.796	1.781	100	0.862	0.114	0.338	3.189	0.309	0.556	1.781
Demospongiae morphotype 4					0.295	20							
Demospongiae morphotype 5	0.048	0.056	0.919	0.466	0.236	100	0.052	$3.165*10^{-5}$	0.006	0.692	0.103	0.320	0.236
Demospongiae morphotype 6			0.031		0.389	40				0.018			0.389
Demospongiae morphotype 7	0.010	0.136	0.512	0.759	0.389	100	0.073	0.008	0.089	0.635	0.031	0.175	0.389
Cnidaria													
Gersemia fruticosa			0.219		2.961	40				0.123			2.961
Amphianthus sp.	0.670	1.069	0.950	2.223		80	0.870	0.079	0.282	1.587	0.810	0.900	
Bathyphellida margaritacea	0.642	0.518	3.582	1.704	0.212	100	0.580	0.008	0.087	2.643	1.763	1.328	0.212

Table 6 (continued)

	1	2	3	4	5	6	7	8	9	10	11	12	13
Annelida													
Polychaeta morphotype 1	0.048	0.024	0.104	0.106		80	0.036	$3.0*10^{-4}$	0.017	0.106	$2.139*10^{-6}$	0.002	
Polychaeta morphotype 2	0.048		0.042	0.067		60	0.022			0.054	$3.0*10^{-5}$	0.018	
Mollusca													
Buccinidae sp.	0.134	0.112	0.115	0.106		80	0.123	$3.0*10^{-4}$	0.016	0.111	$3.506*10^{-5}$	0.006	
Pycnogonida													
Ascorhynchus abyssi	0.488	0.367	0.178	0.133	0.024	100	0.428	0.007	0.086	0.155	0.001	0.031	0.024
Crustacea													
Bythocaris sp.	0.077	0.112	0.261	0.160	0.342	100	0.094	0.001	0.025	0.210	0.005	0.072	0.342
Isopoda indet	0.144	0.199				40	0.172	0.002	0.039				
Amphipoda indet	0.144	0.064				40	0.070	$8.183*10^{-5}$	0.009				
Echinodermata													
Bathycrinus carpenterii	18.432	27.516	3.133	13.325	3.350	100	22.970	41.270	6.424	8.229	51.944	7.207	3.350
Poliometra prolixa	0.881	0.175	1.190	0.466	1.215	100	0.528	0.249	0.499	0.828	0.265	0.512	1.215
Hymenaster pellucidus	0.019	0.088	0.251	0.160	0.083	100	0.053	0.002	0.048	0.205	0.004	0.064	0.083
Poraniomorpha sp.	0.019	0.056	0.073	0.040		80	0.038	0.001	0.026	0.057	0.001	0.024	
Pourtalesia jeffreysi			0.063			20							
Kolga hyalina	0.010					20	0.004						
Elpidia sp.	0.268	0.367	0.188	0.040		80	0.318	0.005	0.070	0.114	0.011	0.105	
Chordata													
Didemnidae indet.	0.153	0.199	0.125	0.439	0.661	100	0.176	0.001	0.033	0.309	0.067	0.260	
Lycode fridigus		0.160		0.040	0.012	60	0.009			0.018			0.012

Table 7. Showing mean density per transect/site, mean densities for all species and biodiversity indices (Shannon-Weaver diversity H and Pielou's evenness J) for each transect/site.

Transect/site	VT6	VT7	VT9	VT10	VT11	Site 1	Var.	±SD	Site 2	Var.	±SD	Site 3
Average depth (m)	2811	2806	2742	2744	2385	mean			mean			
Mean density	24.579	34.559	29.637	33.693	31.261	29.563	24.900	4.990	31.688	4.113	2.028	31.261
Mean densities all species	0.910	1.280	0.847	1.162	0.977	1.095			0.990			0.977
Var.	12.321	27.623	2.210	6.770	3.918	19.630			4.229			3.918
S.D.	3.511	5.255	1.487	2.603	1.979	4.431			2.056			1.979
Diversity indicies												
Shannon – Weaver H	1.241	1.034	2.536	2.151	2.420	1,771			3.046			2.420
Pielou's evenness J	0.377	0.314	0.713	0.640	0.698	0,515			0.850			0.690

3.4.2. *Comparison of faunal communities between sites*

Site 1 had the lowest total no. of observed taxa/morphotypes (31, Table 4, Fig. 17) but the highest recorded no. of organisms (6900, Table 4), with the stalked crinoid *Bathycrinus carpenterii* alone contributing with a recorded no. of 5384 (Appendix, B7). *Site 2* had the highest species richness (36, Table 4, Fig. 17). *Site 2* is composed of more hard substrata than *Site 1* (Table 5), giving more room for hard bottom species to inhabit the area. *Site 2* also had the highest mean density of 31.688 ± 2.0328 ind. m^{-2}, followed by *Site 3* (31.261 ind. m^2) and *Site 1* (29.563 ± 4.900 ind. m^2) (Table 6, Fig. 18).

Fig. 19 shows Shannon-Weaver diversity *H* and Pielou's evenness *J*, for each site, showing *Site 1* ($H = 1.771$, $J = 0.515$), *Site 2* ($H = 3.046$, $J = 0.850$) and *Site 3* ($H = 2.420$, $J = 0.690$). There were significant differences in Shannon-Weaver diversity index between the different sites (p = 0.005). *Site 1* has the lowest *H* and *J* (Fig. 19), having the lowest diversity and the most uneven species distribution. *Site 2* has the highest diversity and the most evenly distribution between species (Fig. 19). *Site 3*, consisting only of one transect (VT11) is less divers than, but closer to *Site 2* regarding both diversity and evenness (Fig. 19). These indices back up the observations of *Site 1* being totally dominated in densities by the crinoid *Bathycrinus carpenterii*, while the other sites are more evenly distributed in densities, being dominated by several species, mainly from the phyla Porifera and Echinodermata (Fig. 20). For instance, the conventionally classified "Encrusting sponge morphotypes 7", is only represented with 18 individuals in the 4 first transects (Appendix, B7), the abundance in VT11 is 907 (Appendix, B6).
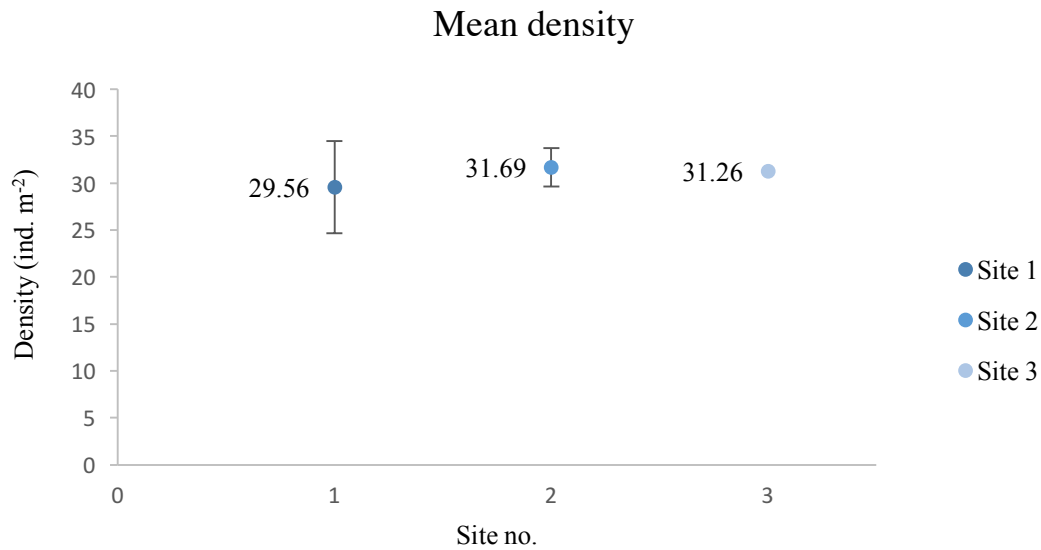
Fig.18. Mean density of species for each site, showing that all sites can be expected to inhabit approx. 30 specimens, regardless of taxa, for each square meter (m^2). The SD for *Site 1* is 4.99 and for *Site 2* 2.03.
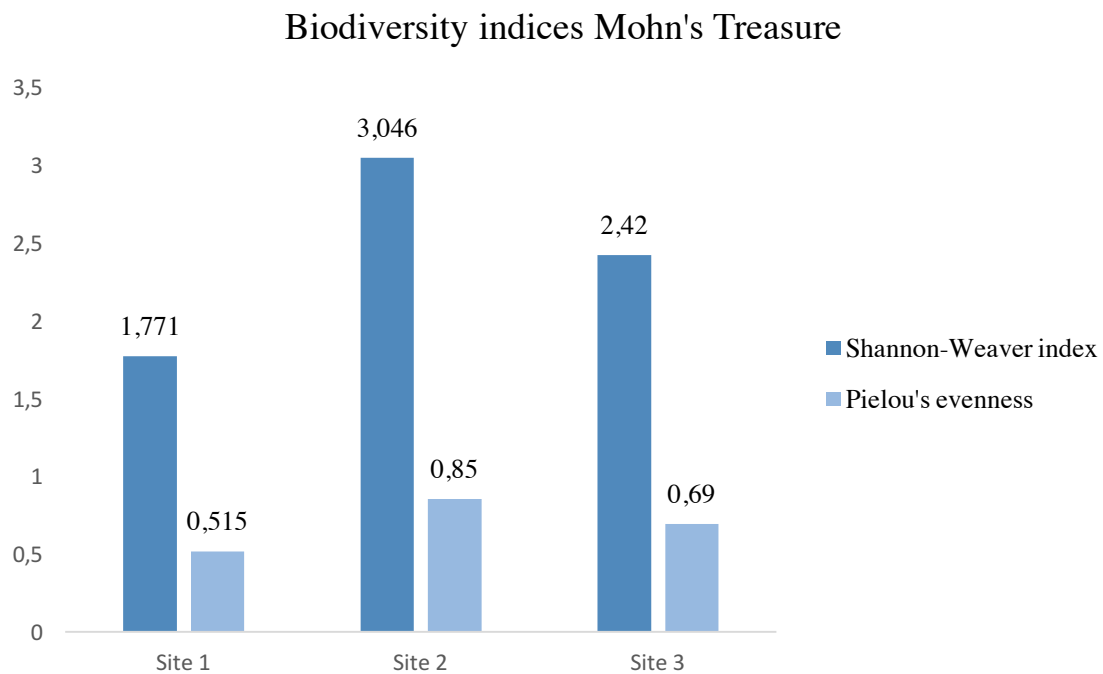
Fig. 19. Shannon-Weaver diversity index *H* and Pielou's evenness index *J* for each site. A higher value of *H* means more diverse. Pielou's *J* can vary between 0 and 1, where 1 is 100% even distribution between species. Showing a more even distribution for *Site 2* than for the other sites.

Mean density per phylum per site
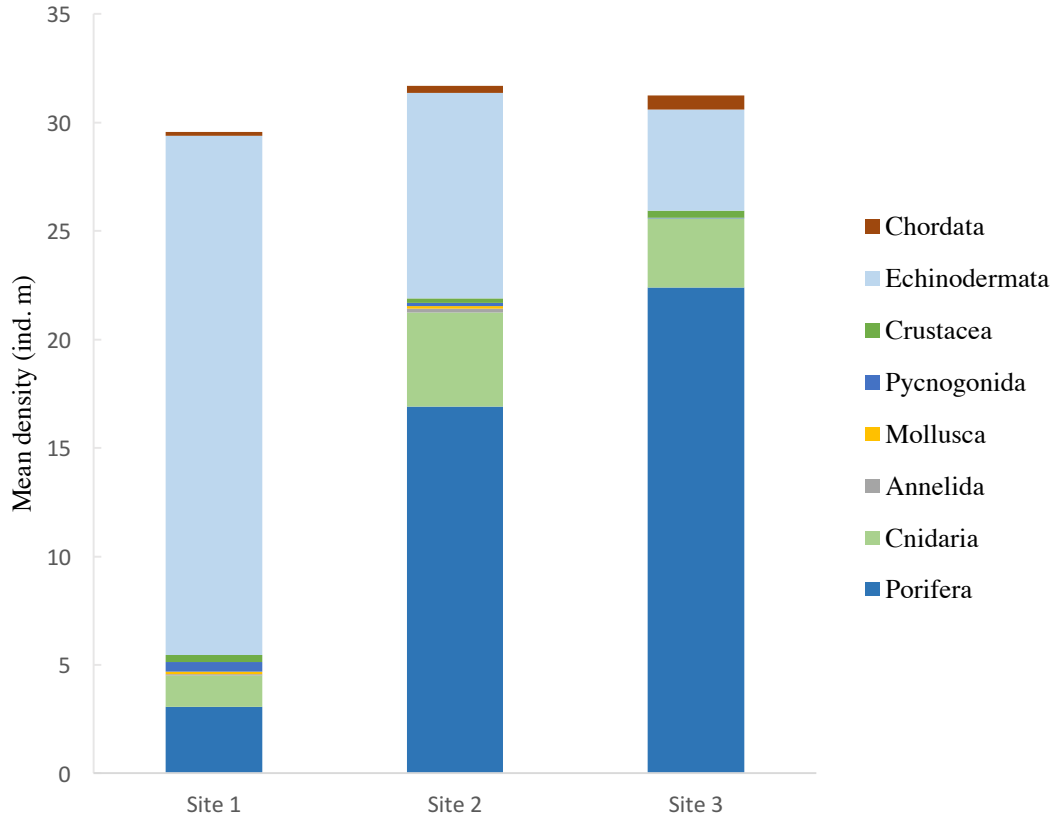
Fig. 20. Showing how the mean density per site is related to the different phyla. The mean density for *Site 1* is dominated by Echinodermata, *Site 3* is dominated by Porifera, while *Site 2* is more evenly distributed between Poriferas, Echinodermatas and Cnidarians.

4. Discussion

This study is the first to investigate the benthic megafauna communities of the deep, geologically inactive vent site of Mohn's Treasure, Mohn's Ridge, AMOR. A total number of 43 taxa have been recorded, and the mean density for each site is approx. 30 ind. m^{-2}. The two most abundant animal phyla, both in number of specimens and number of taxa are Porifera and Echinoderms. The soft sediment is totally dominated by the stalked crinoid *Bathycrinus carpenterii*, while areas of hard bottom substrata is characterised by high abundances of sponges from a large number of species.

This thesis represents a base line study of Mohn's Treasure, and works as an introduction to the megafauna communities inhabiting this location. The data making up the basis upon which this thesis is built comprises of photographs gathered by ROV, piloted from the *CVS Polar King* between the 15th of August and 5th of September, 2016.

4.1. Area covered

For this thesis, the original number of photos conducted during the video transects was 471 (Table 2), with 322 photos having been used for analysis (Tabel 3). As seen in Table 3, the different transects consists of between 52 and 76 photos. As stated in Dias et al. (2015), the task of estimating area of sea bed surface is both challenging and complex. The ROV used for this thesis was equipped with two parallel laser lines 10 cm apart, that could be used to estimate the area of each photograph. Unfortunately, the laser lines contributed to visual pollution in contact with particles in the water, and it was decided to not use laser lines during the transects, but rather take photos with laser lines before the start of each transect. This makes the analysis of the images better, but makes it more difficult to calculate exact square size of the seabed covered in each photograph. This is particularly the case with ROV transects, for which piloting the ROV at a constant distance above seafloor throughout the whole of a transect in variable environmental and topographic conditions is very challenging.

Calculations done with the available information have estimated the sampled area being approx. 230 m^2 for *Site 1*, 170 m^2 for *Site 2*, and 85 m^2 for *Site 3* (Table 3). The reason for *Site 3* being much smaller than *Site 1* and *2*, is mainly because only one transect were could be included in the analysis. The differences in area covered for *Site 1* and *2* on the other hand, both made up of two transects of 200 m, can be explained partly be the altitude of the ROV above

seafloor, which will impact the area per photograph. *Site 1* has the largest mean area per image, with *Site 3* having the lowest (Table 3). In addition, the number of photos analysed from *Site 1* (76) is higher than for *Site 2* (69) (Table 3), leading to differences in site area.

4.2. Taxa recorded

A total of 43 different taxa and morphotypes were observed in the photographs from *Site 1 – 3*, with 15 being identified to species level, 5 to genus level, 4 to family level, 2 to order level and 17 organisms could not be identified further than class. These results represent the first comprehensive study of the Mohn's Treasure, providing a baseline from which to conduct further dedicated studies and sampling addressing specific taxonomic and ecological questions. The limitations in faunal identification in this study were, to a great extend, caused by the relative low resolution of the images. An example is the holothurians in the genus *Elpidia*, which most likely are of the species *Elpidia heckeri*, documented by i.e. Taylor et al. (2017) to inhabit the Fram Strait at similar depths. Nevertheless, the photos do not support accurate identification beyond genus level in this case. In other cases (e.g. some sponges), identification by the use of only images is not possible due to differences at microscopic level, and would require physical sampling. Due to resources limitations regarding time, this thesis has not been able to look at any sampled materials. However, this will be done in the near future.

When identifying species from photographs there is a limitation in size for how small an organisms can be before it is too small to be identified. Based on experience from this study, identification of species under 2 cm can prove very challenging, thus excluding this kind of study of macrofauna (> 0.2mm) and smaller size classes. It may also favour the larger organisms, seeing how they might be easier to identify since they are more easily observed. Nevertheless, the results presented here (Fig. 6) have identified organisms ranging in size from the small sea spider *Aschorychus abyssi* to the arctic eelpout *Lycodes frigidus*. This further indicates that a highly important factor for image analyses of faunal communities from ROV photographs is a sound taxonomical knowledge about local or regional species. For instance, even though the photographs of the sea spider *Aschorhyncus abyssi* does not show any clear taxonomic details, knowledge of its geographic distribution was crucial to be able to identify it to species level (Rapp, unpublished data).

In contrast, identification of cryptic species is highly limited, as certain organisms can have a very similar external morphology but in fact be several different species.

Classification of other unidentified taxa is not only limited by the quality of images, but also by the knowledge of the species found in this area. As pointed out by Rapp (2015) the AMOR ridge (excluding Loki's Castle vent field and Jan Mayen vent field) has mostly never been surveyed with an ROV or sampled biologically. This applies even more to inactive sites in the Norwegian waters, and Mohn's Treasure have remained unstudied up until this study. Because of limited amount of knowledge in the area, several megafauna morphotypes, despite being large enough to be distinguished in the photographic data, have not been identified. The University of Bergen (UiB) has been studying in detail the ecosystem at Loki's Castle vent field (Pedersen et al., 2010), and have also studied the Schultz Massive located next to both Loki's Castle and Mohn's Treasure (Rapp unpublished). However, the studies of these vent sites are still ongoing and the published results focus mainly on the first description of the LCVF (Pedersen et al., 2010), microbiology (Spang et al., 2015; Steen et al., 2016) and on the taxonomy of specific fauna (Tandberg et al., 2011; Kongsrud et al., 2012). This clearly limits the ability to identify all the observed morphotypes from Mohn's Treasure in this purely visual study. What is does indeed do, is emphasize the need of continued work at active and inactive sites along the AMOR.

4.3. Benthic faunal community composition of Mohn's Treasure

The species/taxa accumulation curves for most transects reached the plateau after around 30 photographs, which agrees well with the findings of Taylor et al. (2017) from the Fram Strait. These authors further suggest that 80 photos is sufficient to include the whole taxon inventory. Although in this study only between 52 and 76 photographs were available, the accumulation curves suggest that the sample size was adequate to capture most of the megafaunal taxa present. That being said, it has to be highlighted that VT6 encountered new species around image number 50. When studying the transect in detail, photo 49 – 52 have a different substrata composition than the surrounding images, pointing out the importance of representing all the different habitats in the transect with the images selected for analysis.

When relating the number of photos needed to are size, this indicates that for *Site 1* 220 m^2 should be sufficient to sample the megafaunal community while 170 m^2 would be needed for *Site 2* and 85m^2 for *Site 3*. The plot further shows that most transects stabilized after

approximately 60 m^2 (approx. 70 m^2 for VT6, 55 m^2 for VT7, 60 m^2 for VT9, 50 m^2 for VT10 and 50 m^2 for VT11).

It needs to be mention that, even though this sample size is probably big enough to have recorded most taxa present, a bigger sample size would make the decision even more robust.

4.4. Habitat feature

All sites samples at Mohn's Treasure for this thesis shows a habitat dominated by soft sediment with rocky outcrops. This type of ecosystem is what would be expected at abyssal depths close to a ridge (Ramirez-Llodra et al., 2010). The proportion of soft sand and hard substratum varied between the different sites (Table 5). Although it must be emphasized that this estimation is highly qualitative. It is done purely on the basis of number of photos from the different photo transects which include hard substrata, and compared to the overall number of photos for each transect. This does not have sufficient statistical power to investigate significant differences between the different transects regarding habitat features. Regardless, these indications suggest that the lower slope (*Site 1*) is dominated by soft sediment (approx. 95%, Table 5), and in turn also soft sediment species have the highest abundances. The plateau (*Site 2*) is also dominated by soft sediment (approx. 75 - 80%, Table 5), but also offers considerable areas of hard substratum, including a ridge on the lower area, after which the slope of *Site 1* begins. The upper slope (*Site 3*) is the region with lower proportion of soft sediment (approx. 65%, Table 5), making as much as 35% of the habitat available for hard bottom species.

4.5. Community structure and megafaunal abundances

Mean density for all sites were approximately 30 ind. m^{-2} (*Site 1*: 29.563 ± 4.900, *Site 2*: 31.688 ± 2.0328, *Site 3*: 31.261). *Site 1* had by far the highest recorded number of crinoids, but the lowest diversity (*H* = 1.771), being the least evenly distributes site (*J* = 0.515). *Site 2* were most diverse (*H* = 3.046) and had the most even species distribution (*J* = 0.850). *Site 3* had a diversity index of *H* = 2.420 and evenness index *J* = 0.690).

There three sites studied showed differences in both species richness and abundances. The lower slope had the lowest species richness, with 31 species/morphotypes identified. At the same time, it has the highest overall abundances, totally dominated by the crinoid *Bathycrinus carpenterii*, which highlights the importance of this species at Mohn's Treasure. On the plateau area of Mohn's Treasure, the proportion of rocks and boulders increased,

providing habitat for filter feeders such as sponges. Here high abundances of the sponge *Lyssodendoryx complicata* and *Hymedesmia* sp. were found.

Overall densities for the plateau and upper slope were almost identical, with approximately 31 – 31.5 individuals per square meter. The overall density for the lower slope was also quite similar, with approx. 29.5 ind. m^{-2}.

Shannon-Weaver biodiversity was significantly different amongst the three sites (p = 0.005), with the lowest diversity found on the lower slope (1.771), highest on the plateau (3.406) and intermediate diversity on the upper slope (2.420). The lower slope has the less heterogeneous habitat and is dominated by fields on stalked crinoids, which explains the lower diversity index. The faunal communities at the 3 studied sites had different evenness indices, with the lower slope having the lowest evenness (0,515), the plateau the highest evenness (0.850) and the upper slope intermediate evenness (0.698). These pattern relate to the high dominance of the stalked crinoid *Bathycrinus carpenterii* in the lower slope, and the high species richness on the plateau, with a more evenly distribution of species abundances. Five taxa had all a relatively high abundance on the plateau: *Lyssodendoryx complicate*, *Hymedesmia* sp. Demospongiae morphotypes 3, *Bathyphellida margaritacea* and *Bathycrinus carpenterii*. Even though these taxa are dominating this site, they are not as dominating as *Bathycrinus carpenterii* is in the lower slope, or as dominating as the conventionally classified Encrusting morphotypes 7 is in the upper slope.

When we look closer at *Site 3* we see that there are several species that are represented with between 100 and 300 individuals. This combined with the fact that no species were represented with more than 900 individuals can indicate that this region of Mohn's Treasure is relatively evenly distributed.

4.6. *The benthic megafauna of Mohn's Treasure*

When looking at Mohn's Treasure as a whole, the total recorded species richness is 43. This classification if done on the basis of photographic sampling, with the following limitations. It is not possible to identify all organisms, and for several of the conventionally groups used for quantification, there is beyond doubt more than one species represented. This means that the actual species richness at Mohn's treasure probably is much higher than the numbers presented here. In consultation with experts from UiB, it was decided that it was sufficient and conventional for this study to group similar looking organisms (i.e. sponges). This is on the basis that the phenotypes of these sponges can vary much according to the environmental

factors affecting each individual, and that what may appear as similar organisms in the photographs in fact can be several different species. Schander et al. (2010) report that the sponge fauna from the Jan Mayen vent field area (south AMOR) is characterised by small sponges of the classes Demospongiae and Calcarea. However, the authors indicate that much is unknown about this sponge faunal communities. Identification of the certain species observed in this thesis is difficult simply because description of several of the morphotypes are not yet published or even available. Nevertheless, given the available data, the far most abundant animal group in terms of number of species is the phylum Porifera. They represent 25 of the 43 observed taxa, and constitute 37% of observed organisms. Even though echinoderms are represented with just 7 different taxa, compared to sponges, they still make up 50% of all organisms counted, resulting from the presence of large areas covered by crinoid fields of the dominant stalked crinoid *Bathycrinus carpenterii*, which contributes alone to 47% of the organisms recorded.

This vast fields of stalked crinoid and high abundances of sponges observed at Mohn's Treasure are of significance to potential future deep-sea mining activities. Indeed, whether exploitation of seabed minerals was to take place at an active site such at Loki's Castle or an inactive site such as Mohn's treasure direct impacts from the machinery or indirect impacts from potential sediment plumes could impact these crinoid fields and sponges. But crinoid fields and sponges are included in indicators of vulnerable marine ecosystems (VMEs) by the International Council for the Exploration of the Sea (ICES, 2016) and OSPAR (Hogg et al., 2010). Thus, activities that may cause harm to such communities would need to be strictly regulated and managed (Levin et al., 2016).

5. Conclusion

This MSc thesis represents the first biological study to be done on the geologically inactive site of Mohn's Treasure (AMOR), and aims to describe the community structure and biodiversity of the benthic megafauna inhabiting the area through analysing photographic transects. A total of 43 taxa were observed, with 15 being identified to species level. The different sites studied showed a similar mean density of approximately 30 ind. m^{-2}, with mean densities for all taxa being approx. 1 ind. m^{-2}. The soft sediment was dominated by the stalked crinoid *Bathycrinus carpenterii*, with densities of approximately 20 ind. m^{-2} for some of the transects, while areas of hard bottom substrata is characterised by high abundances of sponges from a large number of species. There were significant differences in diversity between the different sites, with the lowest part of Mohn's Treasure having the lowest diversity, the upper slope had intermediate diversity, while the highest diversity was observed at the middle plateau at approximately 2700m depth. The sites with the highest diversity also had the most even distribution between species.

There are several challenges and limitations faced when investigating benthic megafauna communities using photographic transects gathered using ROV. One issue is the resolution of the cameras being used. This study was originally intended to study video transects. During the cruise it turned out that the resolution of the video camera was not suited for this kind of biological study, and the focus was shifted from video to still photographs (camera type *Kongsberg 14 – 366*). This camera offered images with much higher resolution. With that being said, the camera was unfortunately not HD (high definition), and might have influenced the number of species identified and counted.

Another well-known challenge when surveying the seafloor for biology uses, is the calculation of the covered area size. The ROV used for this cruise was specialised for industrial purposes and not research. Consequences of this was that the laser lines could not be used at all times due to too much interference with particles in the water, and the ROV did not log camera angle. This made the area size calculation more difficult.

A purely visual study like this offers a large number of possibilities and is a great way to study community structure and biodiversity of megafauna. However, the method has its limitations, especially regarding identification of new species. This shows that physical sampling is also needed, and a combination of various research methods might work to supplement each other.

For future work, it is important to continue exploration of the AMOR, to locate and study other active and inactive sites. This is essential in terms of management, particularly in fragmented habitats like vents. Understanding connectivity amongst active vents and understanding the links between inactive sites and the surrounding background habitats is essential to assess resilience of the ecosystems and recovery potential to impact.

6. References

Anja, S., Jimmy, H. S., Steffen, L. J., Katarzyna, Z.-N., Joran, M., Anders, E. L., . . . Thijs, J. G. E. (2015). Complex archaea that bridge the gap between prokaryotes and eukaryotes *Nature, 521*(7551), 173. doi:10.1038/nature14447

Baker, E., & Beaudoin, Y. (2013). In Baker & Beaudaoin (Eds..), Deep Sea Minerals: Sea Floor Massive Sulphides, a physical, biological, environmental, and technical review (p. 5). Vol. 1A, *Secretary of the Pacific Community*.

Baumberger, T., et al. (2016). Fluid composition of the sediment-influenced Loki's Castle vent field at the ultra-slow spreading Arctic Mid-Ocean Ridge. *Geochimica et Cosmochimica Acta* **187**: 156-178.

Brix, S., Meisser, K., Stransky, B., Halanych, K. M., Jennings, R. M., Kocot, K. M. & Svavarsson, J. (2014). Preface – The IceAGE project – a follow up on BIOICE. Polish Polar Research, vol. 35, no. 2, pp 141, 2014

Bouchet, P. & Waren, A. 1979. The abyssal molluscan fauna of the Norwegian Sea and its relation to other faunas. *Sarsia*, 644: 211-243

Dias, F., Gomes-Pereira, J., Tojeira, I., Souto, M., Afonso, A., Calado, A., . . . Dias, F. (2015). Area Estimation of Deep-Sea Surfaces from Oblique Still Images: e0133290. *PLoS ONE, 10*(7). doi:10.1371/journal.pone.0133290

Edmonds, H. N., Michael, P. J., Baker, E. T., Connelly, D. P., Snow, J. E., Langmuir, C. H., . . . Graham, D. W. (2003). Discovery of abundant hydrothermal venting on the ultraslow-spreading Gakkel ridge in the Arctic Ocean. *Nature, 421*(6920), 252. doi:10.1038/nature01351

Fisher, C., Rowden, A., Clark, M. R. & Desbruyéres, D. (2013). In Baker & Beaudaoin (Eds..), Deep Sea Minerals: Sea-Floor Massive Sulphides, a physical, biological, environmental, and technical review (p. 20 - 24). Vol. 1A, *Secretary of the Pacific Community*.

Hogg, M.M., Tendal, O.S., Conway, K.W., Pomponi, S.A., van Soest, R.W.M., Gutt, J., Krautter, M. and Roberts, J.M. (2010) Deep-sea Sponge Grounds: Reservoirs of Biodiversity. UNEP-WCMC *Biodiversity Series* No. 32. UNEP-WCMC, Cambridge, UK.

Høisæter, T. (2010). The shell-bearing, benthic gastropods on the southern part of the continental slope off Norway. *Journal of Molluscan Studies, 76*(3), 234-244.

doi:10.1093/mollus/eyq003

ICES, 2016. ICES Vulnerable Marine Ecosystem (VME) Database Factsheet. 9 pp. Downloaded from:

https://www.ices.dk/marinedata/Documents/VME_FactSheet_ICES_2016.pdf

Kongsrud, J. A., & Rapp, H. T. (2011). Nicomache (Loxochona) lokii sp. nov. (Annelida: Polychaeta: Maldanidae) from the Loki's Castle vent field: an important structure builder in an Arctic vent system. doi:10.1007/s00300-011-1048-4

Levin, L. A., Sibuet, M., Gooday, A. J., Smith, C. R., & Vanreusel, A. (2010). The roles of habitat heterogeneity in generating and maintaining biodiversity on continental margins: an introduction. *Marine Ecology, 31*(1), 1-5. doi:10.1111/j.1439-0485.2009.00358.x

Levin, L. A., Mengerink, K., Gjerde, K. M., Rowden, A. A., Van Dover, C. L., Clark, M. R., . . . Brider, J. (2016). Defining "serious harm" to the marine environment in the context of deep-seabed mining. *Marine Policy, 74*, 245-259. doi:10.1016/j.marpol.2016.09.032

Olsen, B. R., Pedersen, R. B., Rapp, H. T., Thorseth, I. H. & Økland, I. E. (2015). Environmental challenges related to offshore mining and gas hydrate extraction. *Miljødirektoratet*, 2016 **M-532**: 9-16

Oug, E., Bakken, T., Kongsrud, J. A., & Alvestad, T. (2017). Polychaetous annelids in the deep Nordic Seas: Strong bathymetric gradients, low diversity and underdeveloped taxonomy. *Deep-Sea Research Part II, 137*, 102-112. doi:10.1016/j.dsr2.2016.06.016

Pedersen, R. B., et al. (2010). Discovery of a black smoker vent field and vent fauna at the Arctic Mid-Ocean Ridge. *Nature Communications* **1**: 126.

Petersen, S. & Hein, J. R. (2013). In Baker & Beaudaoin (Eds..), Deep Sea Minerals: Sea Floor Massive Sulphides, a physical, biological, environmental, and technical review (p. 8 - 14). Vol. 1A, *Secretary of the Pacific Community*.

Ramirez-Llodra, E., Company, J. B., Sarda, F., & Rotllant, G. (2010). Megabenthic diversity patterns and community structure of the Blanes submarine canyon and adjacent slope in the Northwestern Mediterranean: a human overprint?(Report). *Marine Ecology, 31*, 167.

Ramirez-Llodra, E. (2016). *Exploring arctic vents with Polar King and MarMine team*. MarMine cruise, AMOR.

Rodgers, J. (2013). In Baker & Beaudaoin (Eds..), Deep Sea Minerals: Summary Highlights (p. 4). Vol. 3, *Secretary of the Pacific Community*.

Schander, C., et al. (2010). The fauna of hydrothermal vents on the Mohn Ridge (North Atlantic). *Marine biology research* **6**(2): 155-171.

Sievert, S. M., & Vetriani, C. (2012). Chemoautotrophy at deep-sea vents, past, present, and future. *Oceanography, 25*(1), 218-233. doi:10.5670/oceanog.2012.21

Smith, S. & Heydon, R. (2013). In Baker & Beaudaoin (Eds..), Deep Sea Minerals: Sea-Floor Massive Sulphides, a physical, biological, environmental, and technical review (p. 41 - 44). Vol. 1A, *Secretary of the Pacific Community*.

Snell, J.-A. (1998). A simple benthic sledge for shallow and deep-sea sampling. *Sarsia, 83*(1), 69-72. doi:10.1080/00364827.1998.10413670

Sneli, J.-A., & Wikander, P. B. (2005). *The Marine mollusca of the Faroes* (Vol. 42). Tórshavn: Føroya Fróðskaparfelag.

Steen, I. H., Dahle, H., Stokke, R., Roalkvam, I., Daae, F.-L., Rapp, H. T., . . . Thorseth, I. H. (2016). Novel Barite Chimneys at the Loki's Castle Vent Field Shed Light on Key Factors Shaping Microbial Communities and Functions in Hydrothermal Systems.(Report). *Frontiers in Microbiology, 6*. doi:10.3389/fmicb.2015.01510

Sture, Ø. (2016). "MarMine Cruise Report 2016". NTNU MarMine

Svavarsson, J., Brattegard, T., & Strömberg, J.-O. (1990). Distribution and diversity patterns of asellote isopods (Crustacea) in the deep Norwegian and Greenland Seas. *Progress in Oceanography, 24*(1), 297-310. doi:10.1016/0079-6611(90)90039-5

Sætre, R., Skjoldal, H. R., & Gjertsen, K. (2004). *The Norwegian Sea ecosystem*. Trondheim: Tapir Academic Press.

Taylor, J., Krumpen, T., Soltwedel, T., Gutt, J., & Bergmann, M. (2017). Dynamic benthic megafaunal communities: Assessing temporal variations in structure, composition and diversity at the Arctic deep-sea observatory HAUSGARTEN between 2004 and 2015. *Deep-Sea Research Part I, 122*, 81-94. doi:10.1016/j.dsr.2017.02.008

Van Dover, C. (2010). Mining seafloor massive sulphides and biodiversity: what is at risk? *ICES Journal of Marine Science* **68**(2): 341-348.

Van Dover, C. L. (2014). Impacts of anthropogenic disturbances at deep-sea hydrothermal vent ecosystems: A review. *Marine Environmental Research* **102**: 59-72.

Wille, C., Wille, C., Sars, G. O., & Mohn, H. (1882). *Historisk Beretning ; Apparaterne og deres Brug / af C. Wille : Historical account ; The apparatus, and how used* (Vol. 1:1 2). Christiania: Grøndahl.

Appendix A
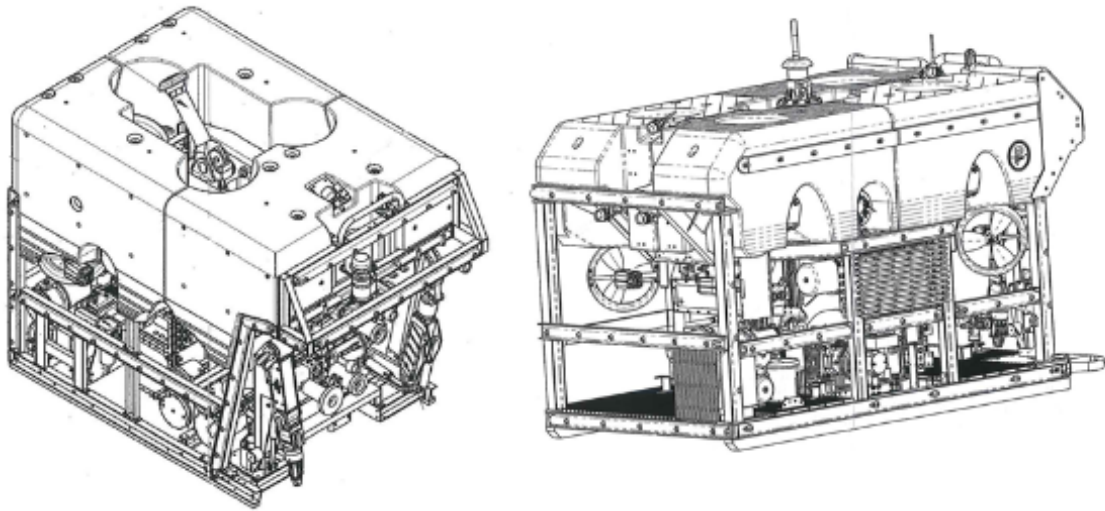
A1. Schematics of the two ROV's, XLR on the left, XLX on the right. Sture, 2016.

Table A2. Standard features *Kongsberg 14-366*

Electrical	
Horizontal Resolution	480 TV Lines (PAL)
Light Sensitivity (Limiting)	0.02 Lux (faceplate)
Scene Illumination	1.7 Lux
Signal to Noise Ration	>48dB weighted (AGC off)
Sensor Type	¼" Interline Transfer CCD with colour Mosaic filter
Scanning	625 Line/50Hz CCIR
Power Output	Constant Voltage 16V – 24V dc, 400mA
Video Output	1.0V Pk – Pk composite video into 75Ω
White Balance	Swith between 3,200K and 5,600K and Auto using the Remote Control
Back Light Compensation	Switch on and off using the Remote Control
Electro-Magnetic Compatibility	EN50081-1 Emossion
Environmental	
Water Depth	3,000 meters
Temperature	Operating -5º to +40 ºC in water Storage -20 º to +60 ºC
Vibration	10g, 20 – 150Hz, 3-axes (non-operating)
Shock	30g pek, 25mS half-sine pulse
Optical	
Standard Lens	4.1mm to 73.8mm, F1.4 – 3
Iris Control	Automatic plus override available with

		Digital control
Focus Control		70mm to infinity (wide angle)
		820mm to infinity (narrow angle)
Angle of View		(1 °)*5.2 ° - 63 ° diagonal in water
		*with Digital Zoom

Mechanical

Diameter	82mm (main body), 95mm (front end)
Length	182mm (excl. connector)
Weight	2.0Kg in Air, 1.0Kg in Water
Standard Housing	Titanium alloy 6AL/4V ASTM B3
Standard Connector	FAWM-8P-BCRA

A2. Showing the method for calculation of square size of images, using input parameters of estimated incline angle of seafloor of 0°, camera angle of 50°, and vert/hor. FOV as respectively 12,75°x17°.

Input		Camera Parameters						Partial Calc					Output						
m	deg	deg	m	pix	pix	deg	deg	m	deg	deg	m	m	m	m	m	mm	mm	mm	m^2
Measured	Estimated incline	Camera Angle	Camera Altitude	Image	Image height	Camera FOV	Camera FOV	Camera	alpha	alpha far	d nea	d far	Swath width horiz	Swath width horiz	Swath width	pixel width	pixel width far	pixel height	Image Area
1	0	50	1,1	2592	1944	12,75	17	2,1	43,6	56,4	2,9	4	0,8671356	1,1335235	1,15621	0,334543	0,43732	0,5948	1,5224

Image projection top row

48

Appendix B

B1. Unidentified objects observed during photographic transects at Mohn's Treasure

SPECIES ABUNDANCES VT6
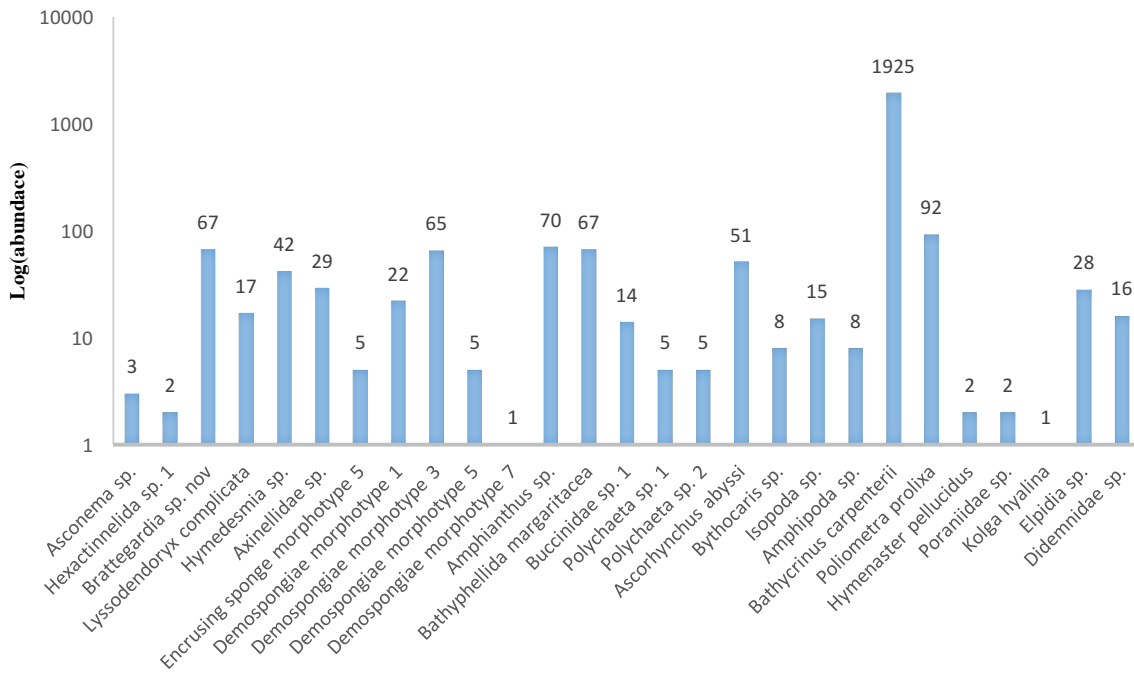
B2. Observed species abundances VT6. X-axis showing the different species/taxa observed at VT6, and y-axis the logarithm of the quantified abundances. This representation is chosen due to immense differences in species abundances between i.e. *Kolga hyalina* and *Bathycrinus carpenterii*.

SPECIES ABUNDANCES VT7

B3. Observed species abundances VT7. X-axis showing the different species/taxa observed at VT7, and y-axis the logarithm of the quantified abundances. VT7 has the single highest recorded abundance of any species in the whole data set, with 3450 individuals of *Bathycrinus carpenterii* on an area covering approx. 125 m^2.

50

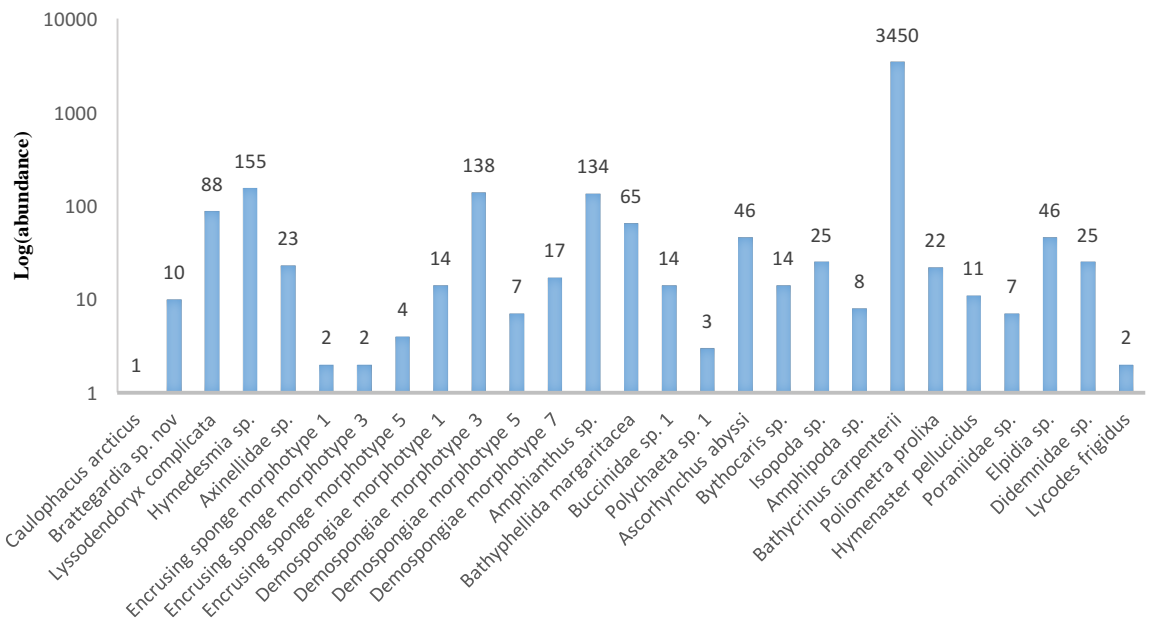# SPEIES ABUNDANCES VT9
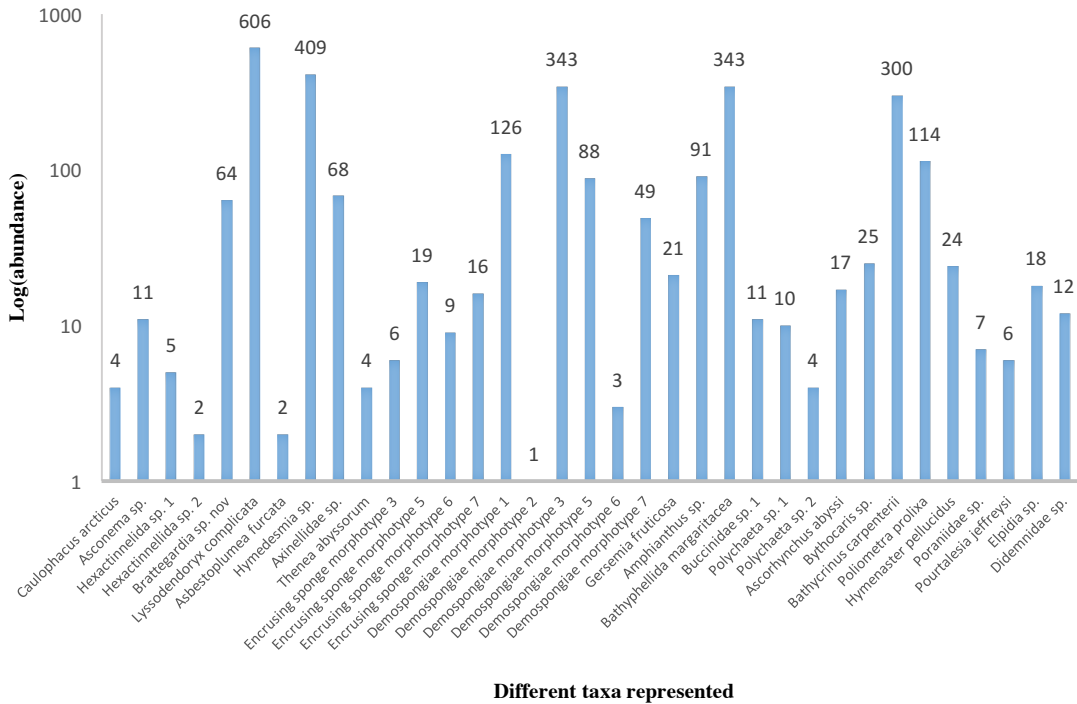
B4. Observed species abundances VT9. X-axis showing the different species/taxa observed at VT9, and y-axis the logarithm of the quantified abundances. The species with the highest abundance is the demospongiae *Lyssodendoryx complicata*, followed by the encrusting genus *Hymedesmia*. The plot also visualizes through no. of bars VT9 being the transect with the highest species richness.
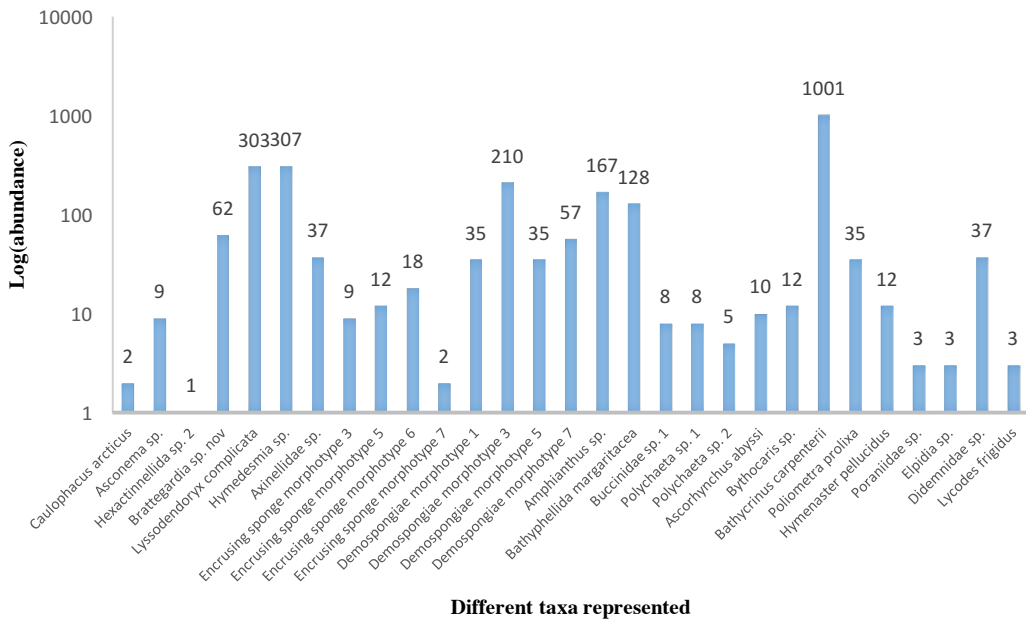
SPECIES ABUNDANCES VT10

B5. Observed species abundance VT10. X-axis showing the different species/taxa observed at VT10, and y-axis the logarithm of the quantified abundances. The plot shows the highest abundance for the cnidarian *Amphianthus sp*. *Amphianthus sp*. attaches to the stalk of *Bathycrinus carpenterii*, and is therefore dependent of its abundance.
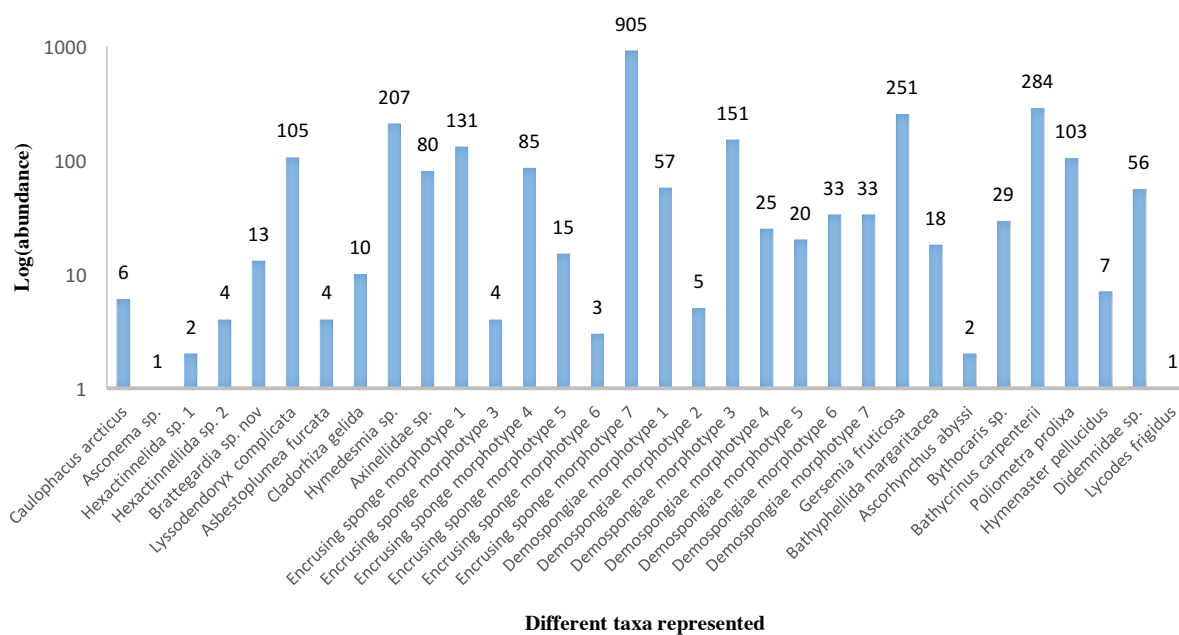
51

SPEIES ABUNDANCES VT11

B6. Observed species abundances VT11/Site 3. X-axis showing the different species/taxa observed at VT11, and y-axis the logarithm of the quantified abundances. The VT is dominated of huge abundances of the small yellow sponge, conventionally referred to as *Encrusting sponge morphotype 7*. It only occurs 18 times at Site 1 and 2, but has an abundance 905 for Site 3

B7. List of different species/morphotypes in taxonomic order and their respective abundances in each transect. Total number shows how many individuals of each taxa that could be recognised in the analysed photos across all transects. The proportion shows to what extend each species/taxa contributes to the total number of organisms at the samples locations, and the frequency shows in how many of the VTs each species is represented.

Transect	VT6	VT7	VT9	VT10	VT11	Total no.	Proportion	Frequency (%)
Depth (m, average)	2811	2806	2742	2744	2385			
Porifera								
Caulophacus arcticus		1	4	2	6	13	$8.71*10^{-4}$	80
Asconema sp.	3		11	9	1	24	$1.61*10^{-3}$	80
Hexactinellida sp. 1	2		5		2	9	$6.03*10^{-4}$	60
Hexactinellida sp. 2			2	1	4	7	$4.70*10^{-4}$	60
Brattegardia sp.*nov*	67	10	64	62	13	216	$1.45*10^{-2}$	100
Lyssodendoryx complicate	17	88	606	303	105	1119	$7.50*10^{-2}$	100
Asbestopluma furcate			2		4	6	$4.02*10^{-4}$	40
Cladorhiza gelida					10	10	$6.70*10^{-4}$	20
Hymedesmia sp.	42	155	409	307	207	1120	$7.51*10^{-2}$	100
Axinellidae indet.	29	23	68	37	80	237	$1.59*10^{-2}$	100
Thenea abyssorum			4			4	$2.68*10^{-4}$	20
Encrusting sponge morphotype 1		2			131	133	$8.91*10^{-3}$	40
Encrusting sponge morphotype 3		2	6	9	4	21	$1.41*10^{-3}$	80
Encrusting sponge morphotype 4					85	85	$5.70*10^{-3}$	20
Encrusting sponge morphotype 5	5	4	19	12	15	55	$3.69*10^{-3}$	100
Encrusting sponge morphotype 6			9	18	3	30	$2.01*10^{-3}$	60
Encrusting sponge morphotype 7			16	2	905	923	$6.19*10^{-2}$	60
Demospongiae morphotype 1	22	14	126	35	57	254	$1.70*10^{-2}$	100
Demospongiae morphotype 2			1		5	6	$4.02*10^{-4}$	40
Demospongiae morphotype 3	65	138	343	210	151	907	$6.08*10^{-2}$	80
Demospongiae morphotype 4					25	25	$1.68*10^{-3}$	20
Demospongiae morphotype 5	5	7	88	35	20	155	$1.04*10^{-2}$	10
Demospongiae morphotype 6			3		33	36	$2.41*10^{-3}$	40
Demospongiae morphotype 7	1	17	49	57	33	157	$1.05*10^{-2}$	100
Cnidaria								
Gersemia fruticosa			21		251	272	$1.82*10^{-2}$	40
Amphianthus sp.	70	134	91	167		462	$3.10*10^{-2}$	80
Bathyphellida margaritacea	67	65	343	128	18	621	$4.16*10^{-2}$	100

B7 (continued)

Taxon						Total		
Annelida								
Polychaeta morphotype 1	5	3	10	8		26	$1.74*10^{-3}$	80
Polychaeta morphotype 2	5		4	5		14	$9.38*10^{-4}$	60
Mollusca								
Buccinidae sp.	14	14	11	8		47	$3.15*10^{-3}$	80
Pycnogonida								
Ascorhynchus abyssi	51	46	17	10	2	126	$8.45*10^{-3}$	100
Crustacea								
Bythocaris sp.	8	14	25	12	29	88	$5.90*10^{-3}$	100
Isopoda indet	15	25				40	$2.68*10^{-3}$	40
Amphipoda indet	8	8				16	$1.07*10^{-3}$	40
Echinodermata								
Bathycrinus carpenterii	1925	3459	300	1001	284	6960	0.467	100
Poliometra prolixa	92	22	114	35	103	366	$2.45*10^{-2}$	100
Hymenaster pellucidus	2	11	24	12	7	56	$3.75*10^{-3}$	100
Poraniomorpha sp.	2	7	7	3		19	$1.27*10^{-3}$	80
Pourtalesia jeffreysi			6			6	$4.02*10^{-4}$	20
Kolga hyalina	1					1	$6.70*10^{-5}$	20
Elpidia sp.	28	46	18	3		95	$6.37*10^{-3}$	80
Chordata								
Didemnidae indet.	16	25	12	37	56	146	$9.79*10^{-3}$	100
Lycode fridigus		2		3	1	6	$4.02*10^{-4}$	60